THERMOELECTRIC PROPERTY STUDY OF N-TYPE PBTE

by

Rico Z. Garza, B.S.

A thesis submitted to the Graduate Council of
Texas State University in partial fulfilment
of the requirements for the degree of
Master of Science
with a Major in Physics
May 2014

Committee Members:

Ravindranath Droopad, Chair

Wilhelmus J Geerts

Tom Zirkle

COPYRIGHT

by

Rico Z. Garza

2014

FAIR USE AND AUTHOR'S PERMISSION STATEMENT

Fair Use

Duplication Permission

DEDICATION

Dedicated to my parents.

ACKNOWLEDGEMENTS

The most important influence on the successful completion of this thesis was the chief technology officer of Micropower Global, Dr. Tom Zirkle. He has had the utmost professional influence on my development as a scientist. He is an amazing scientist and mentor. I am very grateful for his kindness, patience and encouragements, and for allowing me the freedom to work at my own pace.

I want to thank the chair of my committee Dr. Ravindranath Droopad for his limitless support, wisdom, and patience. I also want to thank Dr. Wilhelmus J Geerts, for reading my whole thesis and conveying a lot of valuable criticisms and suggestions. I failed to integrate all of their suggestions, so do not fault them if you disagree with parts of this thesis or find areas in need of revision.

Special thanks to my fellow coworker Dr. Aruna Dedigama for helping me fix the inconsistencies with my understanding of thermoelectrics as well as providing his valuable time and effort to grow the material researched in this thesis. This thesis could not have been done without your expertise.

My mother and father have always been supporting me committedly. They provided me many opportunities in life as well as their unconditional love and support and for that I am thankful. Financial support for this thesis work was provided by Micropower Global.

TABLE OF CONTENTS

Page

LIST OF FIGURES

Figure **Page**

ABSTRACT

In this study, the thermoelectric power density of In-doped PbTe wafers were measured and compared to I-doped PbTe wafers. Both I-doped and In-doped PbTe ingots were grown using a modified vertical Bridgman technique. The crystals were grown in the n-type region of the phase diagram. The I-doped PbTe was doped in order to obtain an electron concentration of $3x10^{19}cm^{-3}$ and the In-doped PbTe was doped at 0.1 at.%. The I-doped PbTe possesses a thermoelectric power density of ~30 W/cm^2 whereas the In-doped PbTe has a power density of ~15 W/cm^2. Despite the In-doped PbTe having a potential almost two times that of the I-doped PbTe, I-doped PbTe possesses a higher initial ZT in the temperature range of 50-450°C along with a normalized power output of almost two times that of the indium doped samples. It is therefore concluded that the use of I-doped PbTe in thermoelectric devices would be greatly preferred over In-doped PbTe from a commercial standpoint.

CHAPTER I

Introduction

1.1 Motivation

As today's energy resources decline, solutions must be found to guarantee the sustainability of the Earth for future generations. To do this in a cost effective manner, minor incremental changes must be made in order to transition to a greener, more efficient and sustainable energy supply. As progress in renewable energy technology continues, it has not yet matured to completely phase out our dependence on oil and coal. Until then, we must continue to develop unique solutions to address the demand for increased energy. One such solution is to capture and convert waste heat generated today by our industrial and transportation sources.

Approximately 80% of the world's energy is generated by fossil fuels. Regrettably, the systems that operate on fossil fuels have an efficiency of~30-40% which results in two-thirds of the energy input being wasted as waste heat. This waste heat is usually produced from power plants, vehicles, appliances, ships, refineries, etc. as shown in Fig. 1. The ability to harvest this waste heat and convert it to electricity would lead to a weaker dependence on fossil fuels. One method that can be used to convert this waste heat to useful power is a thermoelectric module which is shown in Fig. 2. A thermoelectric device uses the temperature gradient, ΔT, between the two ends to generate electricity. It consists of a p-type and n-type thermoelectric material that are linked together and generate power from a temperature difference that exists between T_{hot}

and $T_{cold.}$ The advantage of these thermoelectric generators is that they do not contain any moving parts and are completely silent. These generators have been used reliably for over 30 years of maintenance-free operation in deep space probes such as the Voyager missions of NASA.[1]

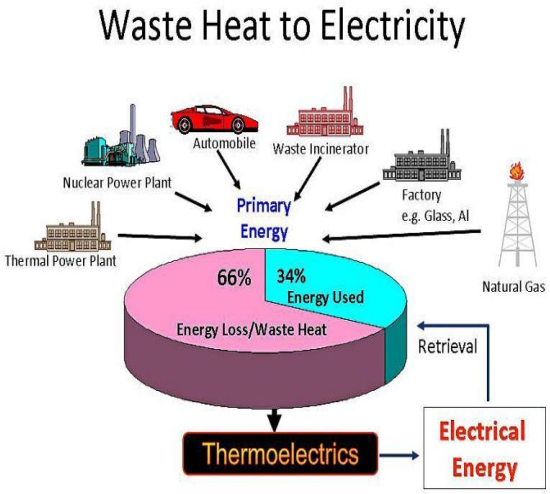

Fig. 1 Sources where most waste heat is given off. Source: www.energy-daily,com

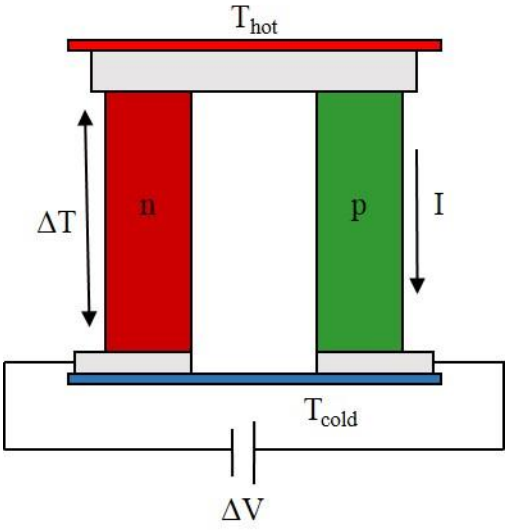

Fig. 2 Thermoelectric module used to generate thermopower.

There are many materials which possess thermoelectric properties. The most widely used thermoelectric materials used today are alloys of Bi_2Te_3 and Sb_2Te_3 and have been studied extensively over the past decade. The efficiency of these thermoelectric materials are heavily dependent on the temperature at which they are used. Bi_2Te_3 and its alloys such as p-type $Bi_{2-x}Sb_xTe_3$ and n-type $Bi_2Te_{3-x}Se_x$ are suitable for use below 400K and are thus the premier materials for thermoelectric generation.[2] For application in the temperature range of 600-900K, PbTe has been proven to be an extremely effective thermoelectric material.

The materials studied in this thesis research are n-type iodine doped PbTe and indium doped PbTe. The performance of "low carrier" indium-doped PbTe are investigated and compared to iodine-doped PbTe. The I-doped PbTe was doped at a concentration of $4.5x10^{19}$ cm^{-3} as determined from the initial mix. On average, this dopant concentration leads to an electron concentration of $3x10^{19}cm^{-3}$ which gives the highest peak ZT in the temperature range of most interest for thermoelectric applications.[3]

The motivation for this research is due to the fact that previous work shows the integrated Z values for PbTe doped with 0.1 at.% In over the 50-450°C temperature range are greater than those of the homogeneous PbI_2-doped samples. Also, In-doped PbTe reaches a potential of ~110mV for a temperature difference, ΔT, of 400ºC.[4] For this voltage, the research of Dashevsky et. al. suggests that with a high current, it is expected that In-doped PbTe could yield a higher power density than that of I-doped PbTe. Part of this result is because as the doping content is decreased for In-doped PbTe, the mobility increases. However, for I-doped PbTe, the mobility increases with increasing doping

concentration. In-doped PbTe also exhibits a unique property which is preferable to thermoelectric application called Fermi-level pinning. Fermi-level pinning is a phenomena when the Fermi level is restricted to lie close to the bottom of the conduction band. As a result, the carrier concentration remains stationary and is no longer dependent on the concentration of indium in the PbTe as seen in Fig. 3. Thus, the impurity level is half-filled, by definition of the Fermi energy, and the electrons from the In-level can annihilate minority carriers and exert beneficial effects. More specifically, the elimination of minority carriers provide a beneficial effect by maintaining the high value of the Seebeck coefficient as a result of the decreasing effect of the minority charge carriers.

In-doped and I-doped samples were prepared according to the stoichiometry and grown using a modified vertical Bridgeman technique. Details on the growth method are provided in chapter 3. The high temperature mobility, carrier concentration, and electrical conductivity of the samples were measured using a van der Pauw system. From the value of the electrical conductivity, the thermal conductivity, in the temperature range 300-600K, was calculated using the Wiedemann-Franz law. A homemade apparatus was designed and utilized to measure the thermal conductivity and Seebeck coefficients in the temperature range of 300-450K. Details of the new instrument are provided in chapter 4. The thermoelectric performance was measured for an 8 cm^3 cubic chip. Results are summarized in chapter 5, followed by a discussion in chapter 6.

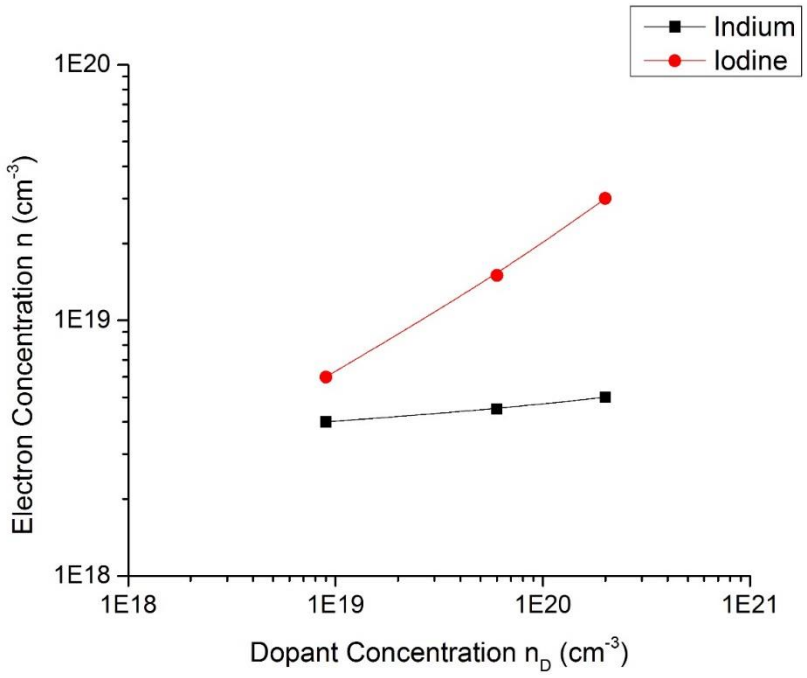

Fig. 3 Electron concentration of iodine and indium doped samples as a function of dopant concentration at T= 300K.[5]

CHAPTER II

Introduction to Thermoelectrics

Thermoelectric devices are based on the Seebeck effect which convert temperature differences into voltage. As mentioned in the previous chapter, this could be used to harness waste heat from industrial and automotive applications into useable electricity. As heat, Q, flows through the device from the hot side, T_h, to the cold side, T_c, electric power, P, is generated. The efficiency of a thermoelectric device, η, is defined as:

$$P = \eta Q \tag{2.1}$$

η depends strongly on the temperature difference, ΔT, across the device. Just like other heat engines, a thermoelectric device cannot have an efficiency greater than that of a Carnot cycle ($\Delta T/ T_h$). The efficiency of a thermoelectric generator can be calculated from the following expression:[6]

$$\eta = \frac{\Delta T}{T_h} \frac{\sqrt{1+ZT}-1}{\sqrt{1+ZT}+T_c/T_h} \tag{2.2}$$

Where ZT is the figure of merit, given by the equation $ZT=S^2\sigma T/\kappa$ where S is the Seebeck coefficient expressed in Volt/Temperature, σ is the electrical conductivity, T is the absolute temperature, and κ is the thermal conductivity. ZT is described in much more detail later in this chapter and is a method for comparing the potential efficiency of different thermoelectric materials. A greater ZT indicates a greater thermodynamic efficiency. In order for thermoelectrics to compete with the efficiency of mechanical

devices and be commercially viable, a figure of merit ZT > 3 is required. Nevertheless, an average ZT of 1.5 to 2 would permit considerable waste-heat harvesting and power generation in certain scenarios such as transportation and military applications. In an attempt to study the efficiency of TE devices and increase ZT, researchers have investigated the decoupling of S, σ, and κ. However, this has been a longstanding challenge as they are strongly integrated with each other through the carrier concentration, phonon scattering, and band structure.[3] As mentioned above, bismuth telluride possesses one of the highest figure of merits, which is marginally above unity at temperature differences of around 100°C. During the last decade, the pursuit for higher efficiency bulk thermoelectric materials has increased. New materials, like quantum-dot superlattices have reported maximum values of ZT > 2.[7]

As can be seen in Fig 4, there are many n-type thermoelectric materials whose efficiencies vary with temperature. The thermoelectric material that is of most interest in this study is PbTe that can be used at temperatures of around 400°C. The figure of merit

peaks around the temperature range T = 400°C-450°C at ZT~1.4.

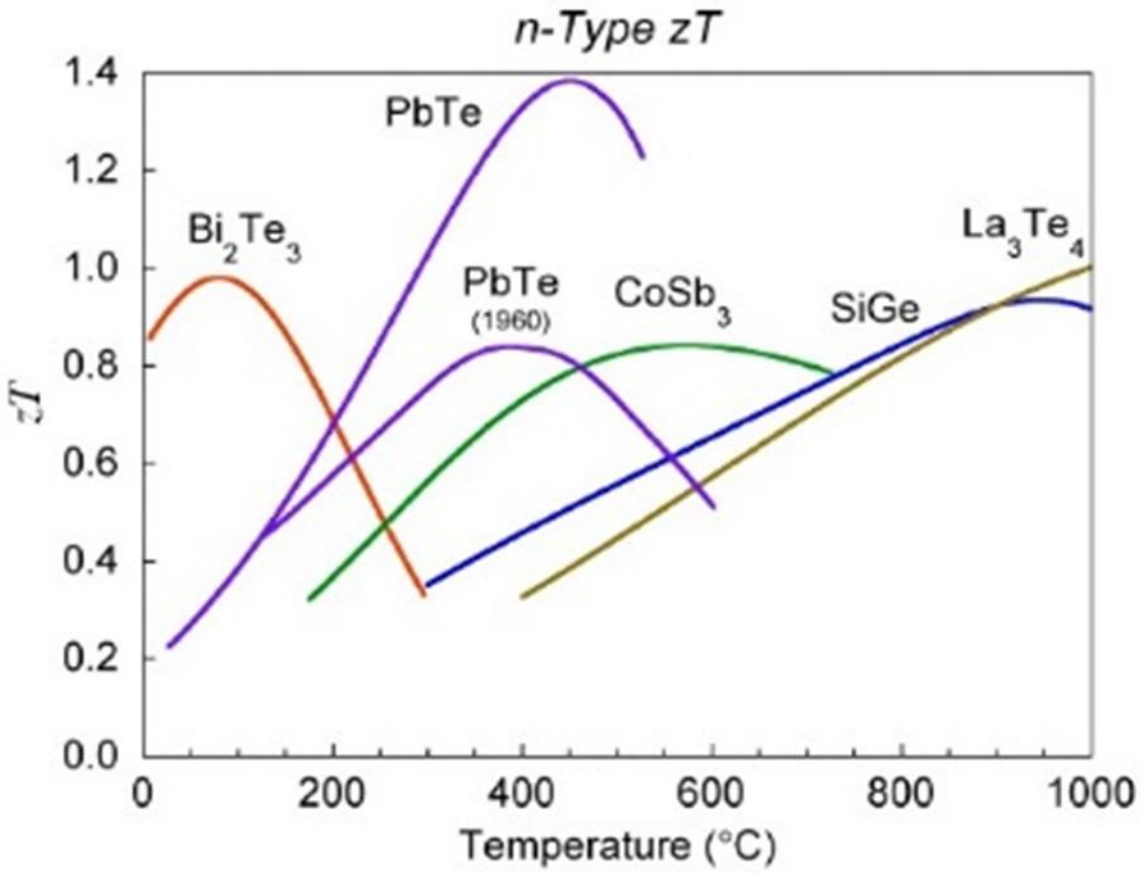

Fig. 4 N-type thermoelectric materials and their respective ZT as a function of temperature**.** Source: http://www.its.caltech.edu/~jsnyder/thermoelectrics/.

2.1 Thermoelectric Phenomena

2.1.1 Seebeck Effect

In 1821 a German physicist by the name of Thomas Johann Seebeck was the first to detect a voltage between both ends of a metal bar in the presence of a temperature gradient along the bar. Later, it was discovered that a compass needle deflected when it was placed near a closed loop formed of two dissimilar metals with a temperature

gradient between the junctions. This demonstrated that a current flowed through the closed circuit that was driven by the temperature difference. The reason for this is that the temperature gradient results in charge carriers (electrons or holes) in the solid moving from the hot side to the cold side. As these charge carriers move, they leave behind their oppositely charged and immobile nuclei at the hot side thus resulting in a thermoelectric potential. Eventually the charge separation creates an electric field which ceases the buildup of charge carriers on the cold side; an equilibrium is established between the diffusion and drift currents. At this point, the material reaches its steady state. Increasing the temperature difference energizes the charge carriers and enables them to continue building up on the cold side thus leading to a higher thermoelectric voltage to which it will once again reach a steady state for that temperature. This thermoelectric potential, or voltage, is also known as the thermoelectric *emf* and is produced by a temperature difference between the two ends of the material. This effect occurs in metals as well as semiconductors. If an external circuit is connected to the thermoelectric device, a continuous net current will flow.

2.1.2 Peltier Effect

The Peltier effect is the converse of the Seebeck effect. Jean Peltier was the first to observe this effect in 1834. This process is the basis used for thermoelectric refrigeration which is currently widely used to cool detectors and manage devices.

When a current passes through a metal and a semiconductor junction, heat is pumped from the junction to the contacts of the device. This results in one end of the

junction heating up while the other end cools off. This depends on the direction of the current. The Peltier effect is shown in Fig. 5.

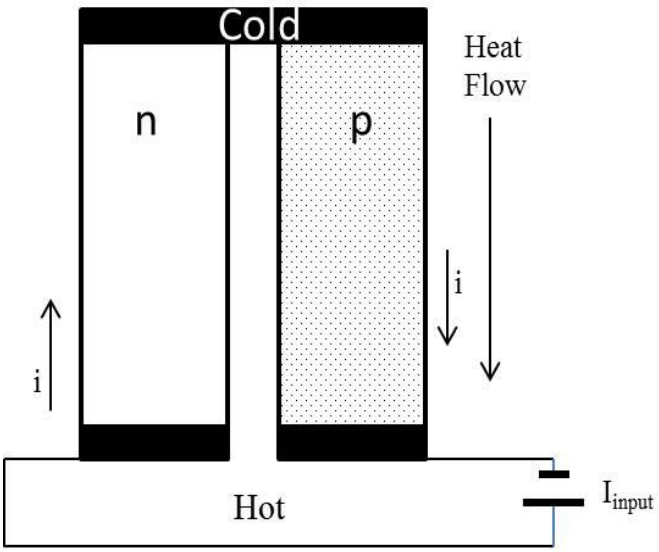

Fig. 5. Description of the Peltier effect with a p-type and n-type module.

2.1.3 Thomson Effect

The Thomson effect is named after the mathematical physicist and engineer William Thomson, whom was later known as Lord Kelvin, in the 1800s. Lord Kelvin was seeking to relate the Seebeck and Peltier effect. He was able to show that heat is liberated or absorbed within a single conductor when an electric current flows through it in the same or opposite direction to the flow of heat. The reversible change in the heat content in a single conductor in a temperature gradient when the current passes through is the Thomson heat.[8]The Thomson effect is defined as the change in the heat content of a single conductor of unit cross section when a unit quantity of electricity flows along it through a temperature gradient of 1 K.[9] In lead, the Thomson effect is roughly zero.

If a current density J passes through a homogenous conductor, the heat flow per unit volume per unit time, q, is given by

$$q = \rho J^2 - \mu J \frac{dT}{dx} \tag{2.3}$$

Where ρ is the resistivity of the material, dT/dx is the temperature gradient along the conductor, and μ is the Thomson coefficient.

The first term in in this is equation,$\rho J^2 = RI^2/V$ represents the produced Joule heat per unit volume per unit time, which is not reversible. The second term,$\mu J \frac{dT}{dx}$, is the Thomson heat. This heat represents energy that is moved to or away from the area by the current. Note that the Thomson heat depends the direction of the current density.

2.1.4 The Thomson Relationship

The Thomson relationship unifies the Peltier coefficient (Π), the absolute Seebeck coefficient (S), and the Thomson coefficient (μ) through the following equation

$$S = \frac{\Pi}{T} \tag{2.4}$$

$$\frac{dS}{dT} = \frac{\mu}{T} \tag{2.5}$$

Note that the Thomson coefficient is zero if the Seebeck coefficient is independent of the temperature

2.2 Thermoelectric Figure of Merit

The dimensionless figure of merit (FOM), ZT, was introduced in the early 1900s by Edmund Altenkirch.[10] The figure-of-merit is known as the standard measure of a materials thermoelectric performance. It incorporated three thermoelectric properties into one mathematical formula. It shows that good thermoelectric materials have a large Seebeck coefficient, high electrical conductivity, and a low thermal conductivity. The large Seebeck coefficient is for maximum conversion of heat to electrical power, low thermal conductivity to retain a large ΔT across the device, and a large electrical conductivity to minimize Joule heating. The regularly used FOM of thermoelectric materials is defined as:

$$Z \equiv \frac{S^2.\sigma}{\kappa} \tag{2.6}$$

where κ is the thermal conductivity, S is the Seebeck coefficient, and σ is the electrical conductivity. It can be seen that Z will have units of K^{-1}, which is why one uses the dimensionless FOM defined as ZT.[3] The numerator of equation 2.4 is referred to as the power factor. It gives the total amount of generated thermoelectric power when the temperature difference across the device is one degree.

2.3 Thermoelectric Performance Optimization

A material with a large thermoelectric power factor, $S^2\sigma$, and therefore ZT, needs to have a large Seebeck coefficient (found in low carrier concentration semiconductors or insulators) and a large electrical conductivity (found in high carrier concentration

metals).[10] For metals or degenerate semiconductors that have a parabolic band and obey energy independent scattering, the Seebeck coefficient is given by:

$$S = \frac{4\pi^2 k_B^2}{3eh^2} m^* T \left(\frac{\pi}{3n} \right)^{2/3} \quad (2.7)$$

Where n is the carrier concentration and m* is the effective mass.[11]

Thus, the power factor is optimized somewhere between a semiconductor and a metal. The electrical conductivity is varied by doping the material, usually with a carrier concentration of 10^{19}-10^{20} carriers/cm^3.

2.4 Thermoelectric Power Generation

Thermoelectric elements generate electrical power from heat based on the Seebeck effect. A basic thermoelectric generator consists of a p-type and n-type leg. In the figure below, the elementary configuration is presented. In practice a module utilizes a number of these p-type and n-type legs usually called couples and are connected thermally in parallel and electrically in a series.

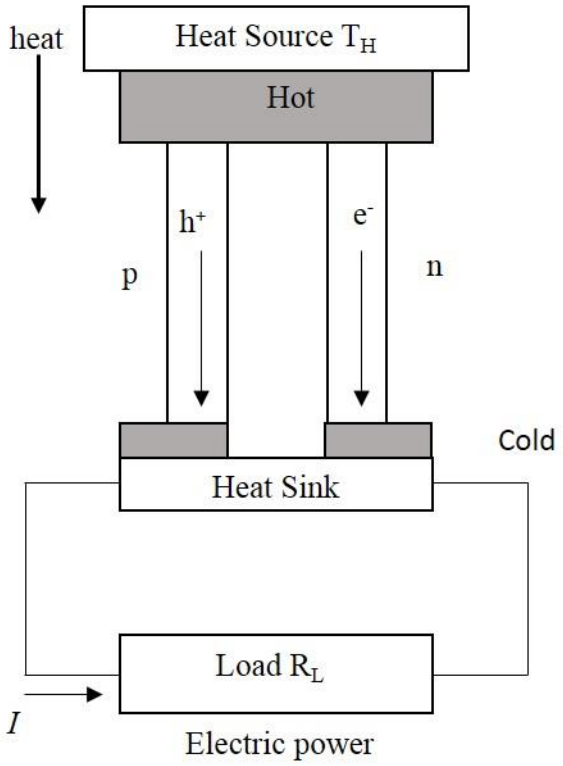

Fig. 6. The two element power generator utilizing the Seebeck effect.

From Fig 6, it is observed that heat flows through the device from the top of the setup and released from the opposite side. In n-type thermoelectric material, the majority of carriers are electrons. In p-type material the majority carriers are holes. Heat flows through the two p-type and n-type from the hot to the cold side of the device. If the device is connected to a circuit of a load resistor, the device creates a current in the circuit and acts like a power generator. The Seebeck voltage produces an electrical current *I* which is proportional to the temperature gradient between the hot and cold junctions ΔT.

$$I = \left(S_p - S_n\right) * \frac{\Delta T}{R+R_L} \tag{2.8}$$

where S_p and S_n are the Seebeck coefficients of the p-type and n-type, respectively, and R is the total electrical resistance of the single couple power generator. The power delivered to the load resistor is given by

$$W = I^2 R_L \tag{2.9}$$

Due to the conduction of thermoelectrics, the heat drawn from the hot junction Q_H is moderately lost. The remainder is used to compensate for the Peltier cooling of the hot junction when a current is flowing through the material.

The conversion efficiency η of thermoelectric power is defined as the fraction of power generated W the thermal power drawn from the input or heat source Q_H. [12]

$$\eta = \frac{W}{Q_H} = \frac{I\left[\left(S_p - S_n\right)\Delta T - IR\right]}{K\Delta T + \left(S_p - S_n\right)IT_H - \frac{1}{2}I^2R} \tag{2.10}$$

In the above equation, K is the total thermal conductance with the n-type and p-type legs in parallel. I, ΔT, S_p, S_n, R, and R_L are the same as they were above.

The figure of merit, Z, of the element generator is directly proportional to the maximum efficiency of the thermoelectric element generator η_{max}. Maximizing the above equation for a chosen R_L, then η_{max} is given by

$$\eta_{max} = \frac{(\gamma - 1) * \Delta T}{(\gamma + 1)T_H - \Delta T} \tag{2.11}$$

where $\gamma = \sqrt{1 + Z\bar{T}}$. Z is the figure of merit and $\bar{T}$ is the average temperature of the hot side, T_H, and the cold side, T_c, $\bar{T} = \frac{T_H + T_C}{2}$. For a single p-n element generator

$$Z = \frac{(S_p - S_n)^2}{K * R} \tag{2.12}$$

where, again, K is the total thermal conductance with p-n legs in parallel and R is the electrical resistance with p-n legs in series. The power generation efficiency η depends on the materials used in the generator, the temperature of the hot and cold side, the electrical resistance, and the load driven by the generator. The maximum efficiency of thermoelectric the thermoelectric power generator, η_{max}, can also be expressed as a function of the Carnot efficiency of a generator $\varepsilon_c (=\Delta T/T_H)$:

$$\varepsilon_C = \frac{\gamma - 1}{\frac{\gamma + 1}{\varepsilon_C} - 1} \tag{2.13}$$

A plot of the power generating efficiencies, η_{max}, as a function of the figure of merit, ZT, for different T_H, and T_c=300K is shown in Fig. 7.

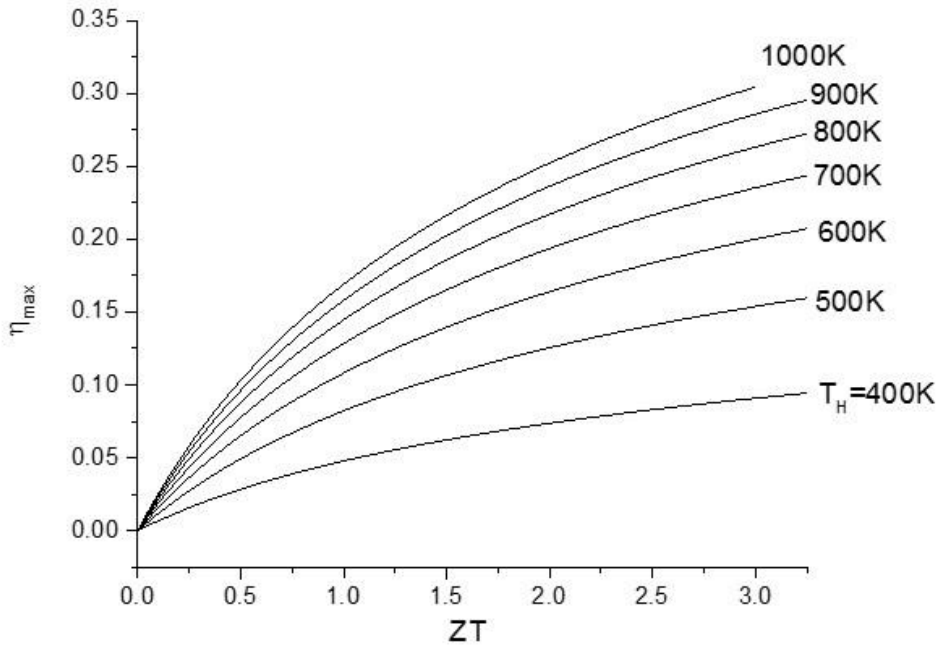

Fig. 7. Power generating efficiency η_{max} as a function of the figure-of-merit for various T_H, and T_C=300K.

2.5 Thermoelectric Cooling

As mentioned above, the Peltier effect is used for cooling. If a current is applied through the thermoelectric couple as shown in Fig. 8, heat is pumped from the hot junction to the cold junction. The temperature of the cold junction will drop below ambient rapidly, provided that the heat is eliminated from the hot side. The temperature gradient will differ according to the amount of current applied to the device.

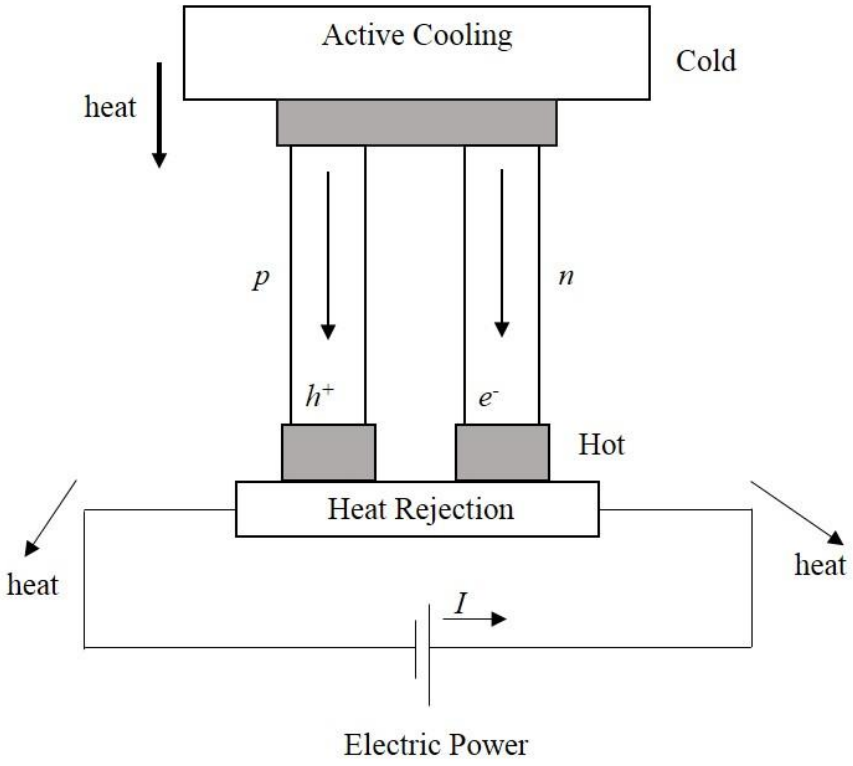

Fig. 8 Single-couple refrigerator utilizing the Peltier effect.

The coefficient of performance, COP, of a heat pump is an indicator of the efficiency of a thermoelectric heater or cooler and is defined as the ratio of the heat pumped by a thermoelectric module and the amount of power consumed to the thermoelectric device. COP offers a measure of performance for heat pumps that is similar to the thermal efficiency for power cycles. The mathematical definition of the COP for a thermoelectric refrigerator φ is

$$\varphi = \frac{Q_C}{W} = \frac{(S_p - S_n)IT - K\Delta T - I^2R/2}{I*[(S_p - S_n)*\Delta T + IR]} \qquad (2.14)$$

Where again, K is the total thermal conductance of the p and n legs in parallel and R is the electrical resistance of the p and n legs in series of a thermoelectric device.

Maximizing the above equation, the maximum COP (φ_{max}) is

$$\varphi_{max} = \frac{T_c(\gamma-1)-\Delta T}{\Delta T(\gamma+1)} \tag{2.15}$$

where $\gamma = \sqrt{1+Z\bar{T}}$. The above equation can be rewritten as a function of the Carnot limit $T_c/\Delta T$ for a refrigerator.

$$\varphi_{max} = \frac{\varphi_c(\gamma-1)-1}{\gamma+1} \tag{2.16}$$

CHAPTER III

Growth and Characterization of Bulk PbTe Crystals

3.1 Lead Telluride

Lead telluride, PbTe, is associated with lead chacogenides which are a group of semiconductors that are composed of an alloy consisting of lead and elements of group VI. Lead telluride and lead selenide are established as good thermoelectrics and remain amongst the most popular thermoelectrics studied. It is a narrow gap semiconductor with a band gap ~.25eV at 0K and .32eV at 300K. The band gap of PbTe has been shown to increase linearly from the temperature range of 0-350K until it reaches a constant value. [13]

PbTe forms a cubic sodium chloride (NaCl) lattice structure. Each Pb (Te) atom is surrounded by six Te (Pb) atoms. PbTe is the face-centered cubic type and the structure is isotropic which means that thermoelectric properties are the same in all directions.

3.2 The Bridgman Technique

Today there are numerous methods used for growing crystals. However, the two most popular methods to grow bulk PbTe are the Czochralski technique and the Bridgman technique. The method that was employed to make the samples reported on in this thesis were made by the vertical Bridgman technique.

The Bridgman technique which is also known as the Bridgman-Stockbarger method is one of the oldest techniques used for growing crystals. The principle of the Bridgman technique is directional solidification by translating the melted constituents from a hot zone to a cold zone. First, the constituents need to be completely melted in the hot zone and be in contact with a seed at the bottom of the crucible. A portion of the seed will be melted by contact of the melt. This offers a fresh boundary for the crystal growth. The seed is a solid piece of the material located at the bottom of the crucible and is used to ensure single-crystal growth along a certain crystallographic orientation.

The Bridgman technique can be implemented into two different configurations. A vertical (vertical Bridgman technique) or a horizontal (horizontal Bridgman technique) configuration can be used. The vertical configuration allows the growth of circular ingots whereas the horizontal Bridgman technique enables the growth of D-shaped ingots. A schematic representation of the vertical Bridgman technique is show in Fig 9.

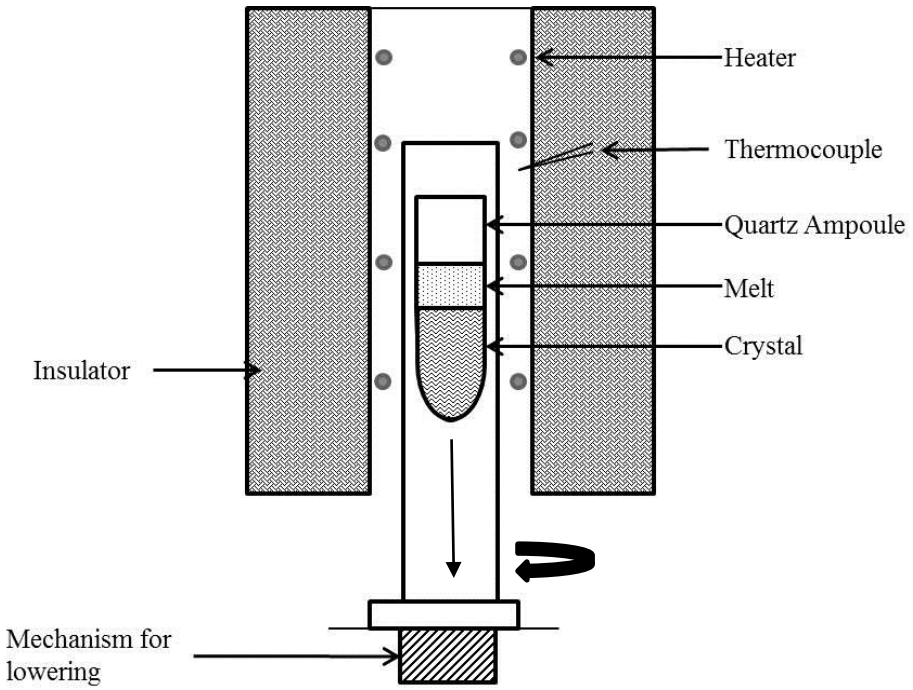

Fig. 9 Schematic of the vertical modified Bridgman apparatus.

From the schematic above, it can be observed that the crucible also rotates as the crystal is being translated. This is to compensate for minor temperature gradients along the horizontal direction.

3.3 PbTe Preparation

A quartz ampoule of 14mm inner diameter (18mm outer diameter) was used as a crucible. The constituents of the ingot were cleaned and then weighed out according to the stoichiometry of PbTe using Pb from ESPI Metals 99.999% purity and Te from 5N Plus which was 6N pure, for the required dopant concentration. All materials were loaded into the quartz ampoule so that during the growth the following reactions take place.

$$Pb + Te + PbI_2 \rightarrow PbTe{:}I$$

$$Pb + Te + In \rightarrow PbTe{:}In$$

Once the materials were loaded into the ampoule, the ampoule was evacuated and then sealed.

3.4 PbTe Growth

The vacuum-sealed quartz ampoule was placed into a rocking furnace that would mix and melt the materials at 900ºC for a maximum of four hours and then was allowed to cool at room temperature. This resulted in polycrystalline materials and also enabled the formation of the seed layer at the bottom of the ampoule.

The ampoule was then loaded into another quartz refractory tube to moderate the influence of external temperature fluctuations and also to allow the translation and rotation of the crystal. The crystal was loaded in a way where the tip of the crucible was outside of the heater and insulation to ensure a solid seed layer. Once the furnace was at the correct temperature, 1020°C, the ampoule began translation from the top. The time taken to grow an ingot was roughly ~8 hours. The PbTe crystal growth flow chart is shown in Fig. 10.

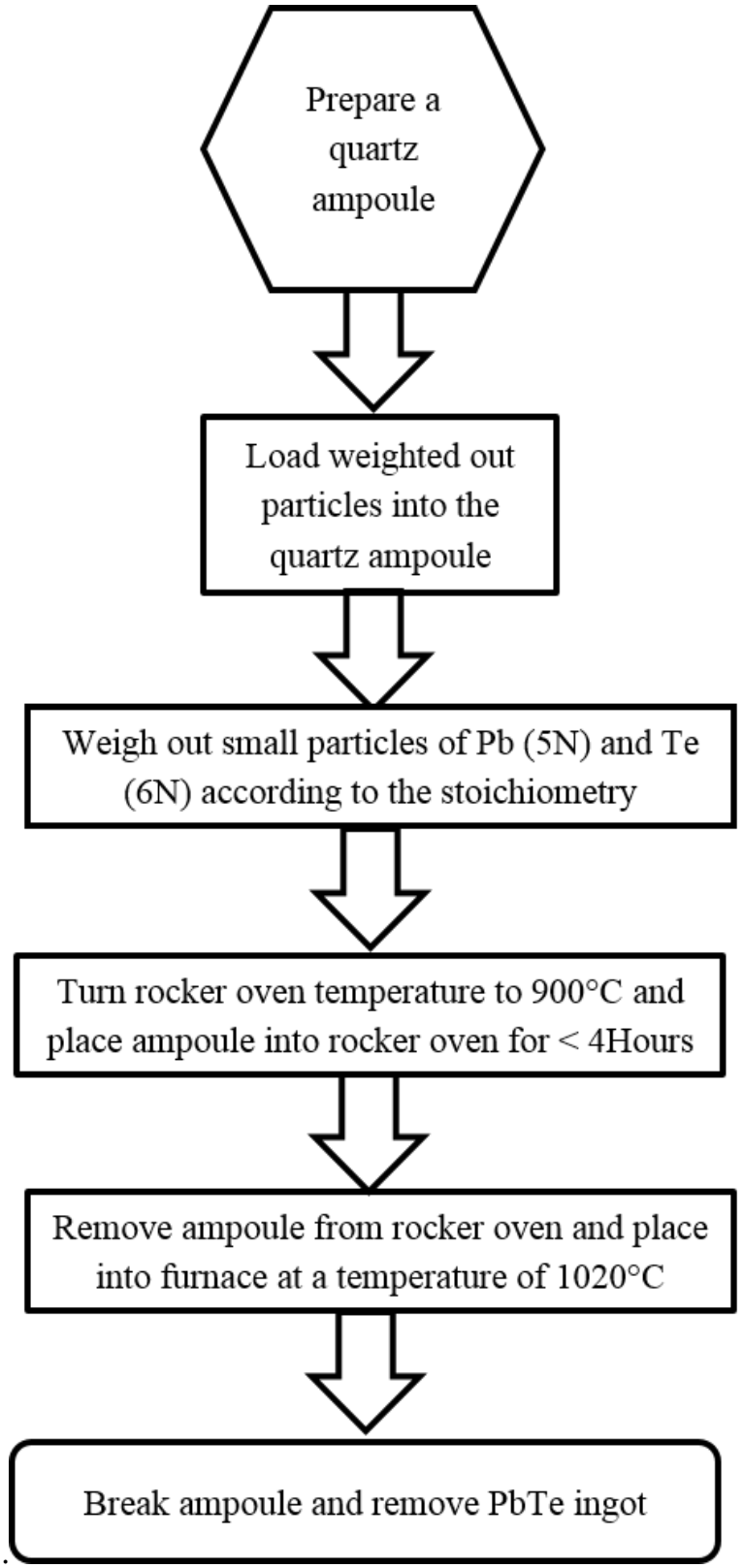

Fig. 10 Flow chart of PbTe crystal growth.

3.5 Wafer Selection

Both the I-doped PbTe and In-doped PbTe ingots were sliced using a diamond saw as shown in Fig. 11. Two wafers from each ingot were chosen to perform measurements to extract the room temperature electron concentration and resistivity. The wafers were placed in the Physical Property Measurement System (PPMS) to determine the electron concentration using a magnetic field of 3T with the resistivity measured using a four point probe.

Fig. 11. Depiction of a sliced ingot and the numbers associated with each wafer.

For I-doped PbTe, a carrier concentration of ~$3x10^{19}cm^{-3}$ was the criterion for selection. This carrier concentration was measured at 3T at 300K using the physical property measurement system, PPMS. This value was particularly chosen because it enables the peak ZT in the temperature range of interest.[3] The respective wafers from the In-doped PbTe were used.

3.6 Physical Property Measurements

After the ingot was sliced, each wafer was cleaned with acetone for ~30 minutes and placed in methanol for 10 minutes to remove the oil from the slicing along with other

impurities. The dimensions of the wafers were measured and recorded. The circular wafers had a diameter of 14mm and a thickness of ~2mm.

The Hall measurements were performed at room temperature using a magnetic field of 0.5T and 3T. The PbTe wafers were loaded onto a Quantum Design® AC transport puck with gold plated pins which enabled Ohmic contacts Fig.12. The carrier concentration (n) was calculated using the relation $n=1/eR_H$, where R_H is the Hall coefficient and e is the fundamental charge of an electron.

Fig. 12 Quantum Design AC transport puck with the gold plated pins.

3.7 Electrical Conductivity

A circular wafer from each ingot was mechanically polished down to 1.5mm and inserted into a four-point probe measurement with a copper probe at the 0º, 90º, 180º, and 270º mark on the wafer. Two copper leads injected a current of 0.5mA through the sample and the other two measured the voltage. The current and voltage leads were switched over all twelve possible configurations with a switching matrix. The four point probe setup was encased in an evacuated metal chamber which allowed uniform temperature throughout the wafer. A Lab View program was created to take Van der Pauw measurements along with varying the temperature of the wafer. A 0.5 mA AC signal was employed at a frequency of 100 Hz in order to cancel out slowly varying (DC) magneto-thermoelectric effects. The Hall measurements were performed at 0.5T. The Hall voltage and the resistivity were measured in increments of 25K starting at room temperature and ending at 600K. From data acquired the carrier concentration and the mobility were calculated. The latter was determined from the carrier concentration and the resistivity results using the equation $n\mu e=\sigma$ where n is the electron concentration, μ is the mobility, and e is the electron charge.

3.8 Thermopower Measurements

An automated device was used to measure the thermopower of the PbTe material. The open circuit voltage and closed circuit current of a PbTe chip was measured and the normalized power density (W/m^2) was calculated for each individual chip. The apparatus consisted of a heat sink that is held at constant temperature via cold water constantly

flowing through the heat sink and a heat source which was a copper cylinder with a diameter of 2” and a height of 2”. A cartridge heater was used to heat the copper cylinder and a K-type thermocouple was placed ~2mm below where the material would be placed. The cylinder was enclosed with insulation and aluminum to ensure a constant and uniform temperature throughout the cylinder. The test was performed under an argon environment to prevent oxidization of the copper and the PbTe material.

The wafer was diced into cubic “chips” with a dimension of 2x2x2mm. The wafer was cut using a diamond saw after which and the chips were cleaned with acetone and methanol. Before the test, the dimensions of each chip were measured and then a thin layer of Ga-Sn eutectic was placed on opposite ends of the chip to ensure sufficient contact between the heat source and the heat sink. The chip was then loaded onto the center of the copper cylinder ~2mm above the thermocouple to ensure an accurate temperature reading. It has been theorized that compression of thermoelectric, specifically PbTe, materials result in a decrease in the band gap which would yield enhanced performance.[9] The compression also ensured that the sample made full ohmic contact, with the help of the GaSn eutectic, to both the heat sink and the heat source to provide more accurate data. The program then ran power through the cartridge heater and an open circuit voltage and closed circuit current was measured at 40ºC and in 20ºC increments to 440ºC.

From circuit theory, given a generator, the maximum power output is obtained by matching the external load resistance to the internal source resistance which occurs at a 50% efficiency.[15] To calculate the power given from a thermoelectric element, we introduced a field-effect transistor gate, FET gate, which at a certain voltage bias,

controls the resistance. As the resistance is increased, the current density and the power density are recorded and the maximum power is obtained by taking the maximum value of this curve.

3.9 Thermal Conductivity

Thermal conductivity, κ, indicates the ability of a material to conduct heat, Q, in time *t* through a thickness of a material L, due to a temperature difference, ΔT in a direction normal to the cross-sectional area A. This, of course, is under steady state conditions and when the heat transfer depends on the temperature gradient only. The quantity κ can be expressed as:

$$\kappa = \frac{Q}{t}\frac{L}{A\Delta T} \tag{4.1}$$

The total thermal conductivity of a semiconductor represents the transport of heat by phonons (the lattice thermal conductivity), free electron or holes (the electronic thermal conductivity), photons, i.e., electromagnetic radiation, and electron-hole pairs in the intrinsic conduction region. [16] To measure the thermal conductivity of the samples a special measurement setup was developed that is described in Chapter 4. The system was also used to measure the Seebeck coefficient.

CHAPTER IV

Thermal Conductivity and Seebeck Apparatus

4.1 Design of Thermal Conductivity Apparatus

Measurement of thermal conductivities, κ, for semiconductors is usually difficult to implement as a result of a low thermal conductivity of the material under test. Since κ for thermoelectric materials is typically quite low, and other "parasitic" heat flows can be similar in magnitude to the thermally conducted heat and can cause significant errors. [16]

The apparatus in Fig 13 was designed and built to measure the thermal conductivity along with the Seebeck coefficient. During measurement, the complete test fixture was enclosed in a vacuum to prevent heat losses from convective heat.

The thermocouples along with the nichrome heating wire went in through the sidewalls of the apparatus. To avoid shorting the nichrome along with avoid giving false temperature measurements, a ceramic double bore tube with an outer and inner diameter of 0.094" and 0.025" respectively was placed in the holes of the apparatus as depicted above. The nichrome filament was a 24 AWG wire and was used as a radiative heat source to create a small temperature gradient throughout the material to measure the Seebeck coefficient, which will be discussed later. A 0.5" outer diameter ceramic cartridge heater was placed through the bottom hole and was used to heat the entire

apparatus from 300K to ~475K. The rationale for not allowing the system to achieve a temperature >475K was due to the fact that the solder used to hold the thermocouples and wires to the tabs would eventually become soft leading to a disconnection. Also, the insulation for the silver-coated copper wire could not exceed 200°C.

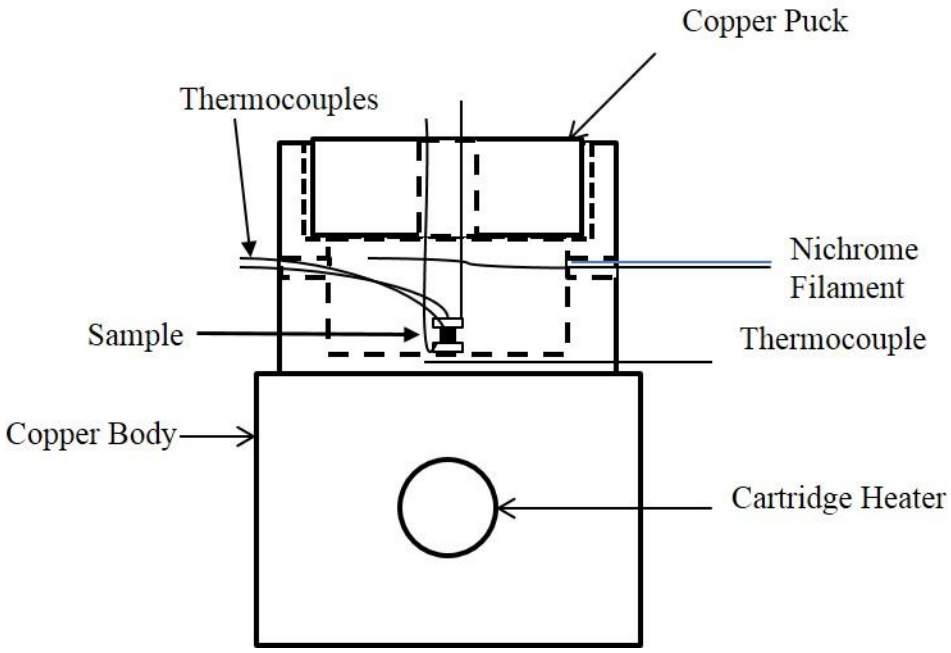

Fig. 13 Thermal Conductivity and Seebeck apparatus.

Resting at the bottom of the apparatus was a PbTe chip with dimensions of ~2x2x2mm with two Ni tabs soldered to the top and the bottom of the material. The opposite ends of the chips were Ni plated and the Ni tabs were soldered onto the chip using 7N indium. Each nickel tab was ~6mm in length 2mm wide and 0.5mm in height. Ni was chosen as the contact material because of its high thermal conductivity. A 0.003" K-type thermocouple and a 28 AWG silver-coated insulated copper wire was soldered onto each nickel tab using high temperature solder. This wire allowed current to be

injected along with the capability to measure the potential difference across the material. The wire went through the top of the apparatus while the thermocouples avoided the nichrome filament and departed out through the sidewall of the apparatus, as mentioned above, to prevent shorting out the thermocouples along with damaging the thermocouple insulation. Before being soldered to the nickel tabs, the thermocouples were calibrated using boiling deionized water.

The schematic of the PbTe chip along with the Ni tabs is shown in Fig. 14 and a photo of the setup is shown in Fig 15.

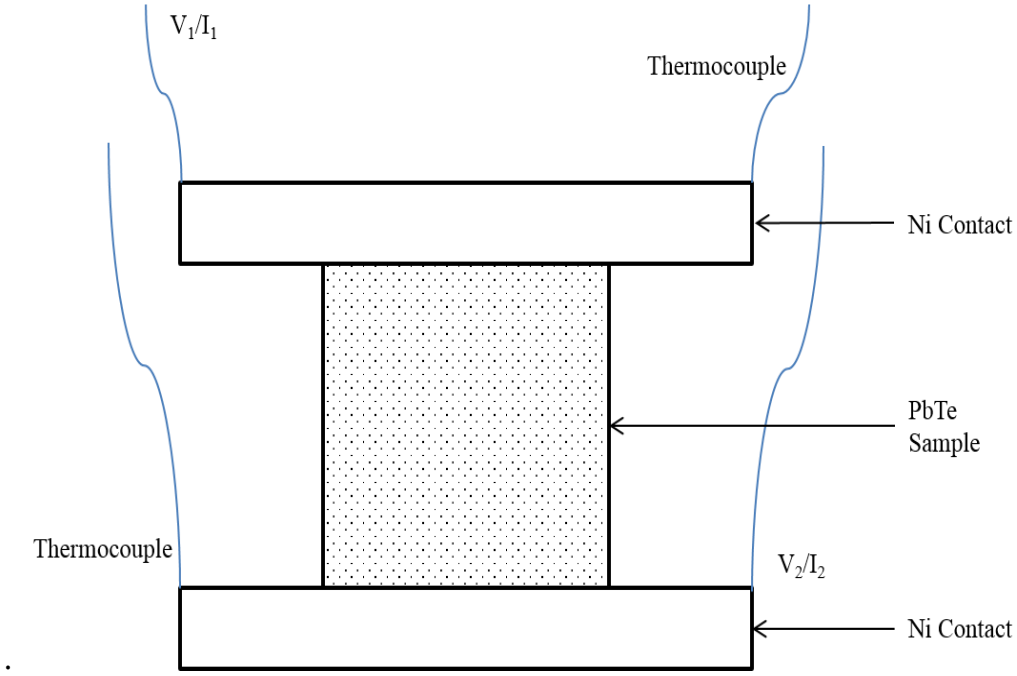

Fig. 14 Schematic of the Ni contacts on a PbTe sample.

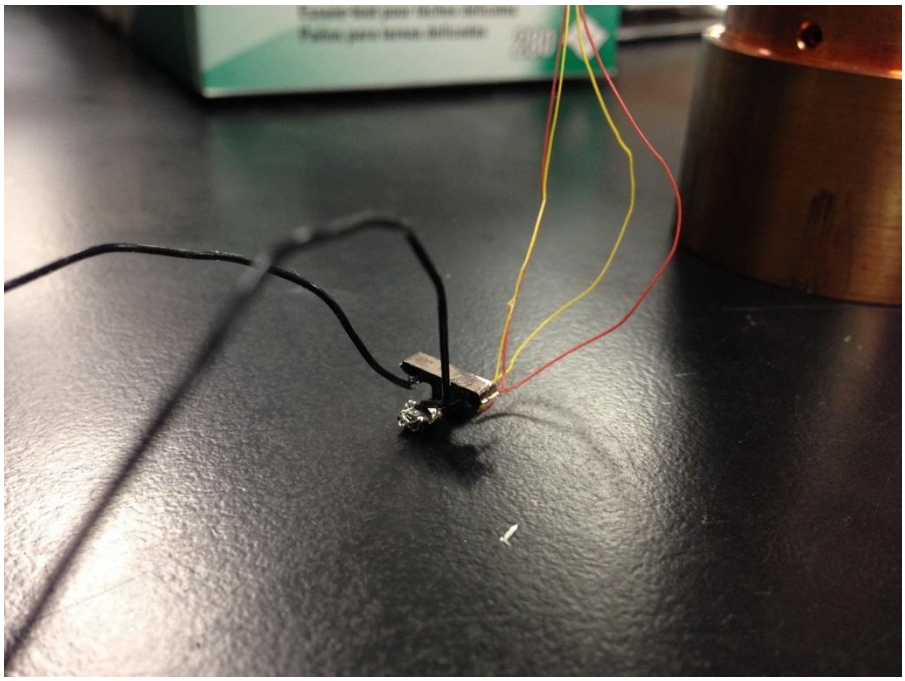

Fig. 15 PbTe "chip" with attached thermocouples (blue and yellow wires) and the wires needed to measure potential difference (black).

4.2 Seebeck Coefficient

The Seebeck coefficient S, also called thermopower, is related to the electronic structure. In general, the sign of the Seebeck coefficient specifies the dominant charge carrier type. N-type materials encompass a negative S whereas the p-type materials have a positive S. The two wires V_1 and V_2 were connected to a Keithley digital multimeter to measure the open circuit DC voltage throughout this measurement. The thermocouples were connected to an Omega thermometer which measured the temperature difference across the PbTe material. The setup above was placed in a copper cylinder and was held in place by double sided graphite tape. While graphite tape was thermally conductive it was electrically insulating. The copper cylinder was then heated to 40ºC, based on the

thermocouple in the copper apparatus, and the measurements were made in increments of 20ºC.

Once the sample was isothermal, current was injected through the nichrome wire which was located ~1mm above the top Ni tab. The radiative heat from the nichrome wire increased the temperature of the top nickel tab to produce a slight temperature difference, ΔT, ~3ºC. After this condition was met, the ΔT and the corresponding Seebeck voltage, ΔV (=V_c-V_H), of the chip was measured. Using the following equation

$$S = \lim_{\Delta T \to 0} \frac{\Delta V}{\Delta T} \tag{5.1}$$

the Seebeck coefficient was able to be computed at each temperature.

Since the distance from the edge of the chip to both thermocouples was ~1.5mm the Seebeck coefficient from the Ni tabs must be accounted for. To account for this it was determined that a small correction of $12x10^{-6}$/K was subtracted from the measured voltage. The purpose for subtraction is because the thermoelectric emf of nickel has a negative value.[17] This is the same value expected from n-type thermoelectric materials.

4.3 Thermal Conductivity

When the apparatus described above was enclosed in a vacuum, the relevant heat flows that contributed to the PbTe sample were the radiative Stefan-Boltzmann, Q_{SB}, Peltier heat, Q_{Π}, the thermally conducted heat Q_{κ} the radiative heat loss, $Q_{radiation\text{-}error}$, and

the parasitic heat flows from the connected wires, Q_{wires}. At steady-state, the sum of the heat flows must converge to zero.

$$\sum Q = Q_{SB} - Q_{\Pi} - Q_{\kappa} - Q_{radiation-error} - Q_{wires} = 0 \quad (5.2)$$

When Q_{SB} is applied by the nichrome heater, the temperature of the cold contact will begin to increase and the heat will be conducted through the sample. If the temperature across the sample, ΔT, is less than 10K, $Q_{radiation\text{-}error}$ and Q_{wires} in 5.2 can be negated [17] giving:

$$\sum Q = Q_{SB} - Q_{\Pi} - Q_{\kappa} = 0 \quad (5.3)$$

The Peltier heat flow, Q_{Π}, is given by the following equation [15.18]:

$$Q_{\Pi} = SIT \quad (5.4)$$

where S is the Seebeck coefficient, I is the current, and T is the temperature. The equation for the thermally conducted heat, Q_{κ}, is:

$$Q_{\kappa} = \kappa(\frac{A}{l})\Delta T \quad (5.5)$$

where κ is the thermal conductivity of the material, A is the area of the sample, and l is the height of the sample. Solving equation 5.3 for Q_{SB} and taking the derivative of ΔT with respect to current gives the following equation:

$$\frac{\partial \Delta T}{\partial I} = \frac{STl}{\kappa A} \quad (5.6)$$

As a result of the low thermal conductivity of PbTe, the temperature of the contact which was adhered to the carbon tape is greater than the temperature of the contact close to the nichrome heater. The sample was made isothermal by applying Q_{SB} and was verified by measuring the potential difference across the sample. When the chip and the contacts were completely isothermal and equaled the temperature of the copper apparatus, the nichrome filament was used to apply a small temperature difference across the sample. Once a ΔT of about 3°C was acquired, a discrete DC current was applied to the sample. The slope of the change in temperature, ΔT, with respect to discrete set of current values, *I,* was recorded and plugged into equation 5.6. With the dimensions and prior knowledge of the Seebeck coefficient, the thermal conductivity can be calculated.

CHAPTER V

Results and Discussion

5.1 Iodine Doped PbTe

Three wafers from a single ingot were characterized to determine their thermoelectric properties. These wafers showed to have an electron concentration of ~$3x10^{19}cm^{-3}$ at room temperature determined with the PPMS using a magnetic field of 3T. The resistivity of each wafer was~.4Ω-cm.

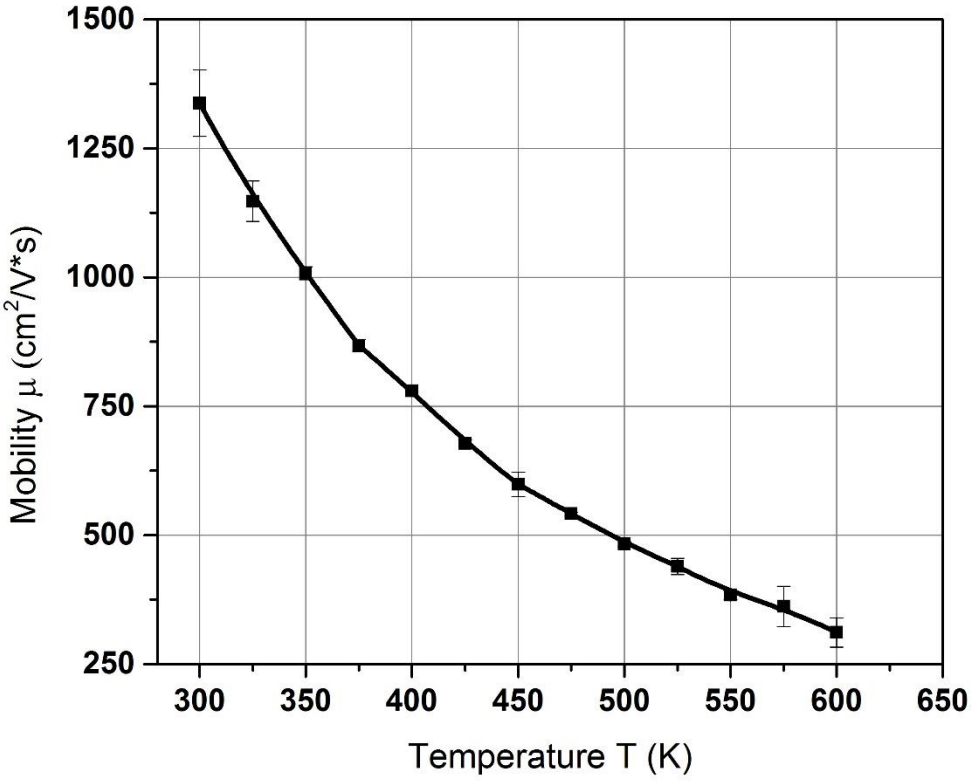

Fig. 16 Mobility of I-doped PbTe as a function of temperature.

Fig. 16 shows the calculated mobility of these three wafers as a function of temperature. The mobility initially starts off at ~1340 $cm^2/(V*s)$ at 300K and decrease to a value of ~600 $cm^2/(V*s)$ at 600K. A decrease in the mobility could be accounted for due to an increase in phonon scattering as the temperature increases. The influence of impurity scattering, due to the amount of iodine introduced into the PbTe material, could also play a larger part in affecting the mobility at higher temperatures.

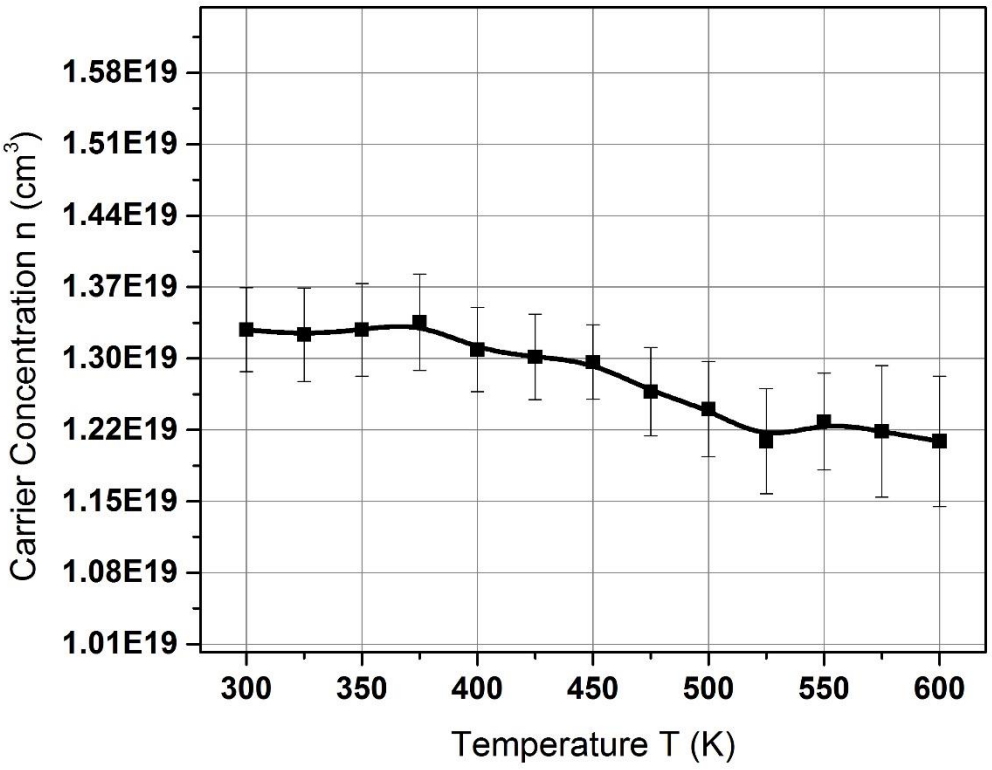

Fig. 17 Electron Concentration of I-doped PbTe as a function of temperature.

Fig. 17 shows the calculated Hall electron concentration as a function of temperature. As the temperature rises, the number of ionized minority carriers is increased thus leading to the slight drop in the electron concentration.[19]

Using the values from Fig. 16 and Fig.17 the equation $n\mu e=\sigma$, can be used to calculate the electrical conductivity, σ. Since the mobility decreases, it should be expected that the electrical conductivity also decreases which can be observed in the following Fig. 18.

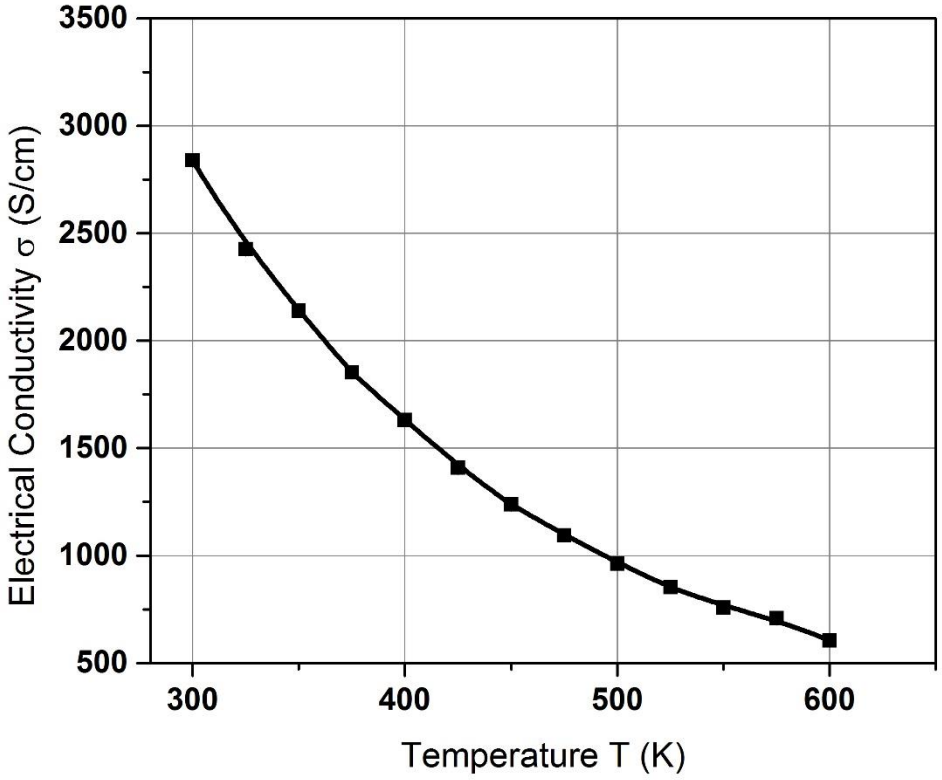

Fig. 18 Electrical Conductivity of I-doped PbTe.

As a result of the decrease in electrical conductivity, the thermal conductivity should be affected as well. The thermal conductivity and the electrical conductivity are related by the Wiedmann-Franz law:

$$\frac{\kappa}{\sigma} = L_0 T \qquad (6.1)$$

where L_0 is known as the Lorenz number for a non-degenerate sample and T is the temperature. A non-degenerate semiconductor is a semiconductor for which the Fermi energy is at least 3kT away from the band edge. Since the material examined is heavily doped with iodine, we can then assume that the Fermi level is close to the conduction band. The Lorenz number is constant [20] and its value for PbTe is 2.45×10^{-8} W Ω K^{-2}. Using the above relation, the thermal conductivity is calculated and is shown in the following figure.

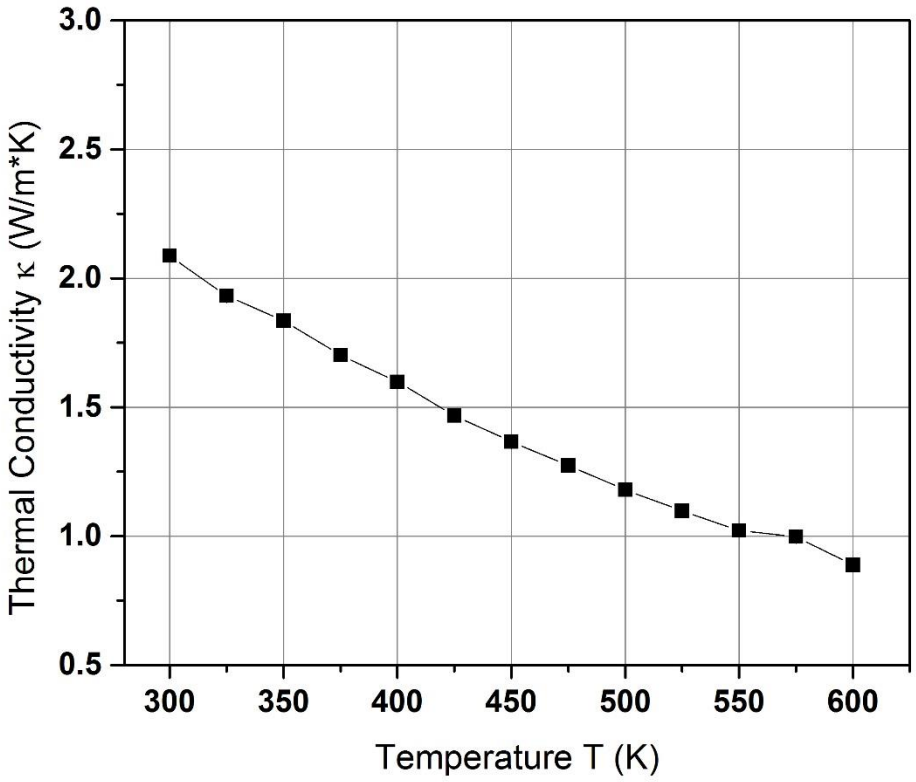

Fig. 19 Calculated thermal conductivity of I-doped PbTe as a function of temperature.

It was observed that the thermovoltage of the iodine-doped PbTe material is linearly increasing with temperature. The open circuit voltage monotonically increases and reached a measured value of ~66mV with an error of ±0.57mV at 440°C.

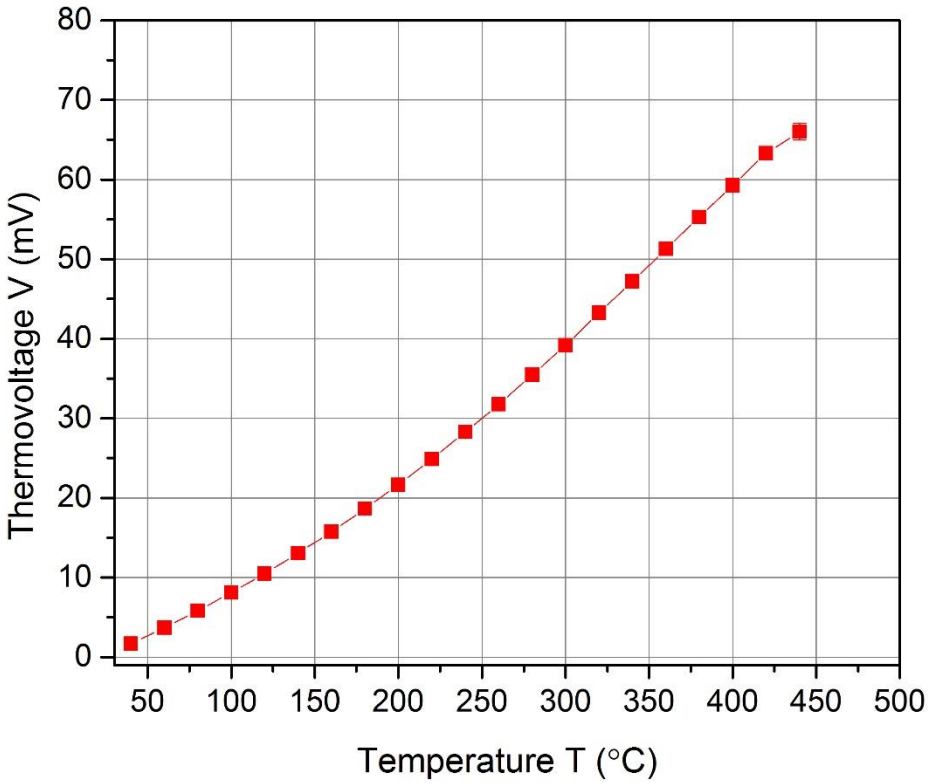

Fig. 20 Thermovoltage as a function of temperature for I-Doped PbTe.

From the voltage and its corresponding current, we could compute the average power density, P_D, of the two PbTe cubes (W/cm^2). The computation is as follows:

$$P_D = \frac{I_{cc} h V_{oc}}{10wd} \tag{6.2}$$

where I_{cc} is the closed circuit current at a certain temperature, V_{oc} is the corresponding open circuit voltage, h is the height (distance between hot and cold junctions), the 10 is a result of unit conversions, w is the width, and d is the length of the PbTe chip. It can be seen that the power density is normalized to a 1mm height chip.

The power density for I-doped PbTe calculated from (6.2) is given in Fig. 21. Upon examination, it seems that the power density would continue to rise past the temperature limitation of the thermoelectric test apparatus. Note that the power density is expected to increase beyond where the peak ZT occurs.

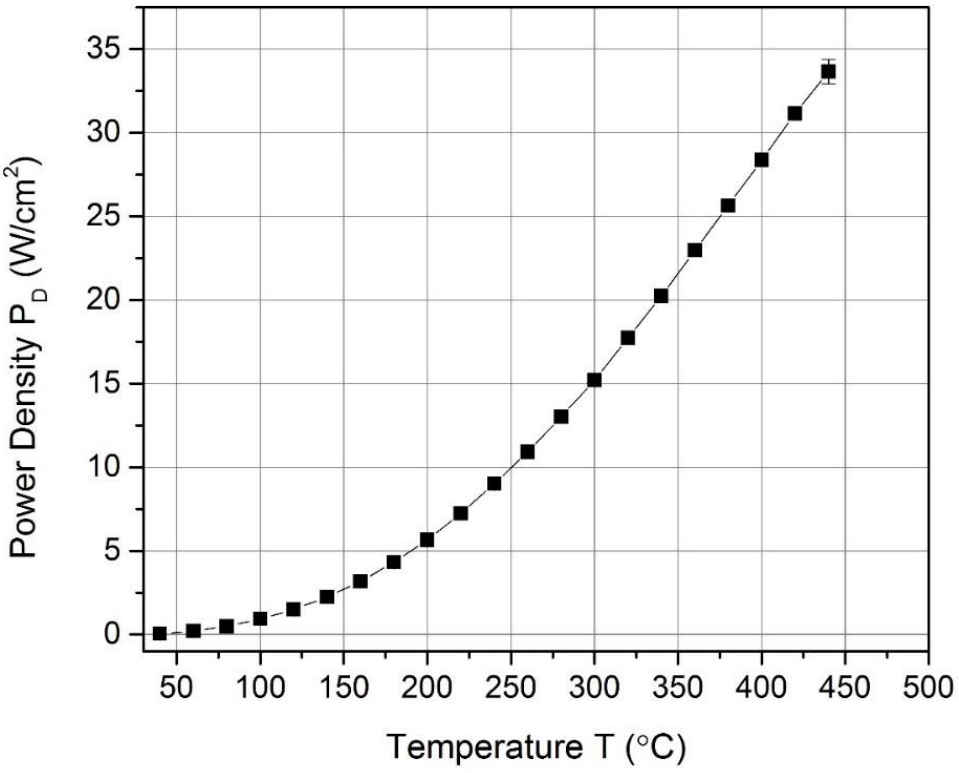

Fig. 21 Power density of I-doped PbTe.

It is observed that the power density, P_D, of the I-doped sample increases exponentially and reaches a normalized power density of ~33W/cm^2 at 440°C.

5.2 Indium Doped PbTe

PbTe was doped with In to 0.1at.% because it was previously found that the Z values for In-doped PbTe over the temperature range 50-440°C was higher than those for I-doped PbTe but slightly lower than those of the optimally graded I-doped PbTe.[5] The reason for not increasing the dopant concentration was because the In-doped sample, in contrast to the I-doped sample, exhibit an increase in the electrical resistivity as the doping concentration increases. The measured electron concentration reaches a saturation point around (3-5)x10^{18}cm^{-3}.This is illustrated in Fig. 22 which shows the electron concentrations throughout an In-doped PbTe ingot that was doped at 2.9x10^{20}cm^{-3}, or 0.3 at. % In. These measurements were performed at room temperature in a magnetic field of 3T.

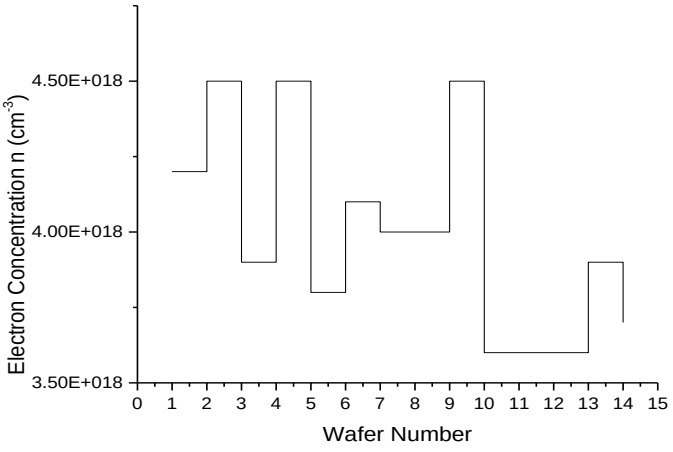

Fig. 22 Electron Concentration for In-doped PbTe 0.3at.% In at 0.5T vs. the corresponding wafer number.

It's observed that the average electron concentration is ~$4x10^{18}cm^{-3}$ and the second, fourth, and ninth wafer possessed the highest measured carrier concentration with a concentration of $4.5x10^{18}cm^{-3}$. This is good agreement with the statement mentioned earlier implying a saturation level at $(3\text{-}5)x10^{18}cm^{-3}$. This saturation level is a demonstration of the Fermi level pinning effect in In-doped PbTe.

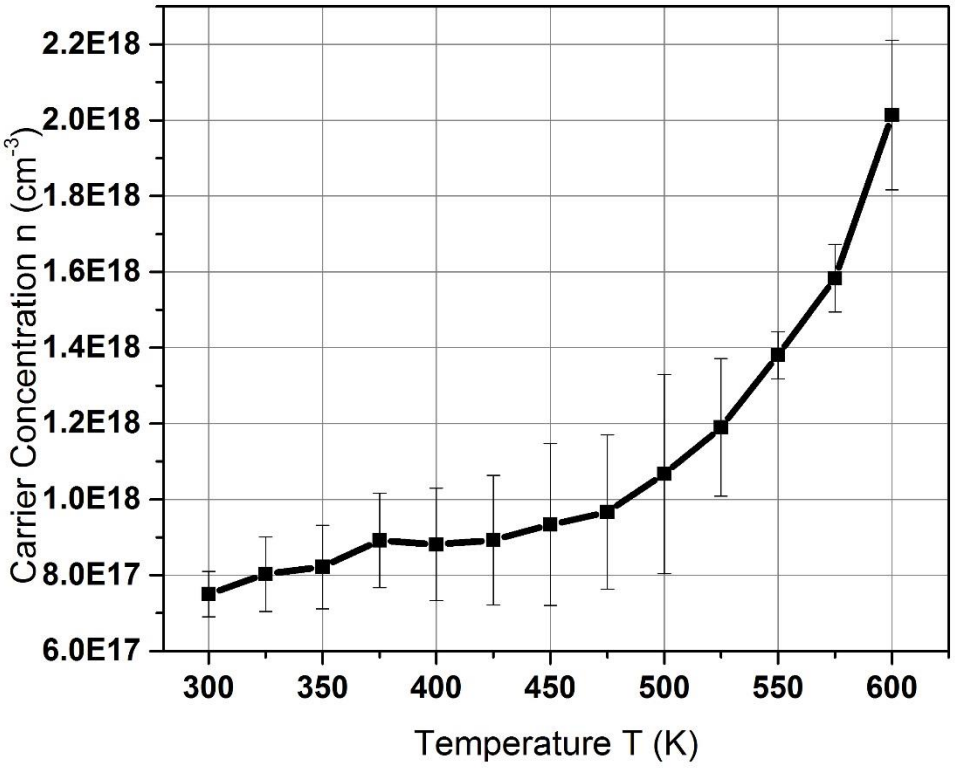

Fig. 23 Electron Concentration of In-Doped PbTe as a function of temperature.

It is witnessed in Fig. 23 that the electron concentration increases with temperature. This is expected for semiconductors since the carriers have increased energy to be thermally activated into the conduction band. However, the I-doped sample did not

exhibit this characteristic and its electron concentration remained the same as temperature increased. The initial carrier concentration of the In-doped PbTe at room temperature is ~$8x10^{17}cm^{-3}$ in a magnetic field of 0.5T and increased to ~$1.8x10^{18}cm^{-3}$ at 600K

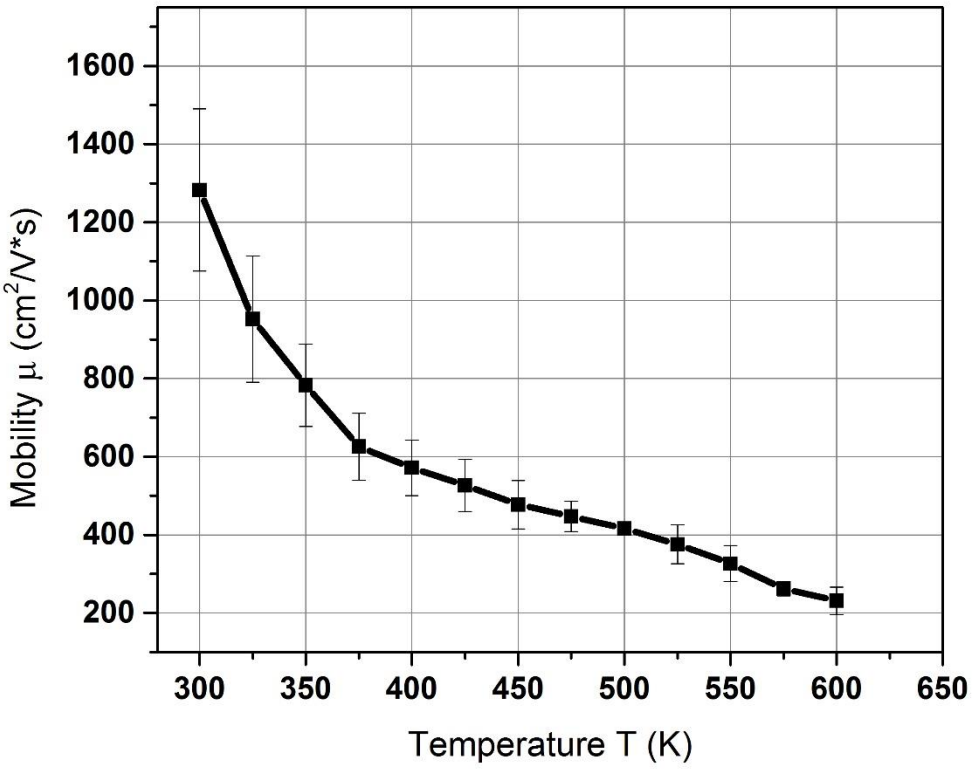

Fig. 24 In-Doped PbTe mobility as a function of temperature.

In the figure above, the variation in mobility is similar to the I-doped sample in which also decreases. The In sample rapidly decreases from ~$1050cm^2/Vs$ at 300K to ~270 cm^2/Vs at 600 K. Both combining the electron concentration with the mobility, the electrical conductivity is acquired and is shown in Fig. 25. The electrical conductivity

falls quite rapidly and appears as if the electrical conductivity levels off around the 450K mark and averages around 85 S/cm.

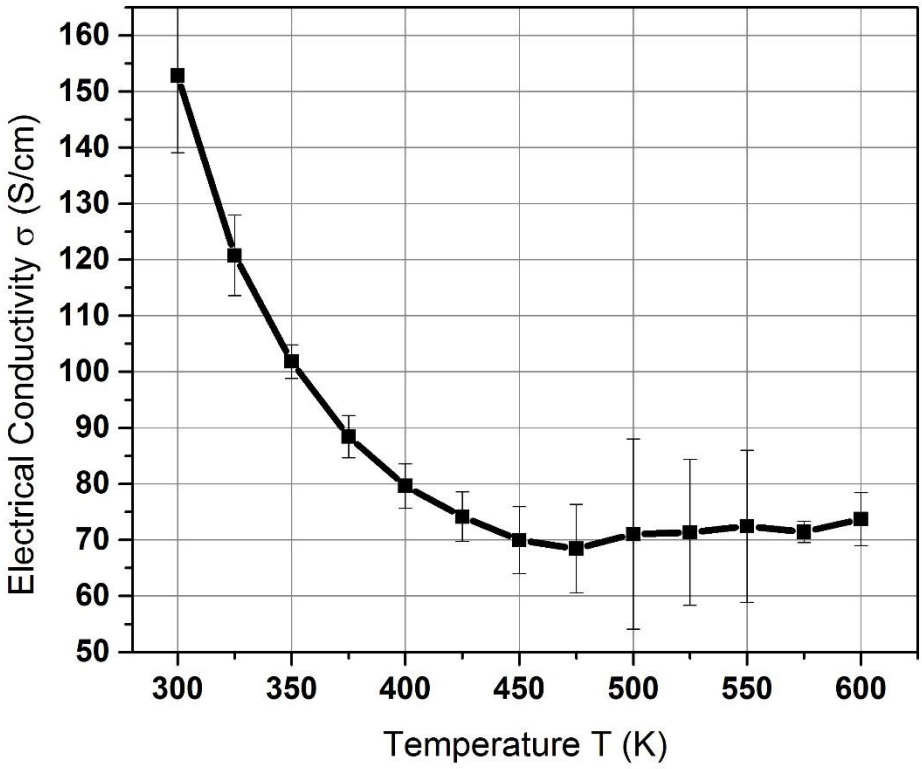

Fig. 25 Electrical Conductivity of In-doped PbTe.

The thermal conductivity of the 0.1at. % In-doped sample is computed the same as the I-doped sample. From the Wiedmann-Franz law, the thermal conductivity should also decrease due to the linear relationship with the electrical conductivity. Fig 24 shows the calculated thermal conductivity from the measured electrical conductivity along with the errors associated with the electrical conductivity measurement. It is observed that the shape of the graph is quite unique however; the thermal conductivity varies from 0.0083-

0.012 W/m*K which is a small change compared to that of the I-doped PbTe.

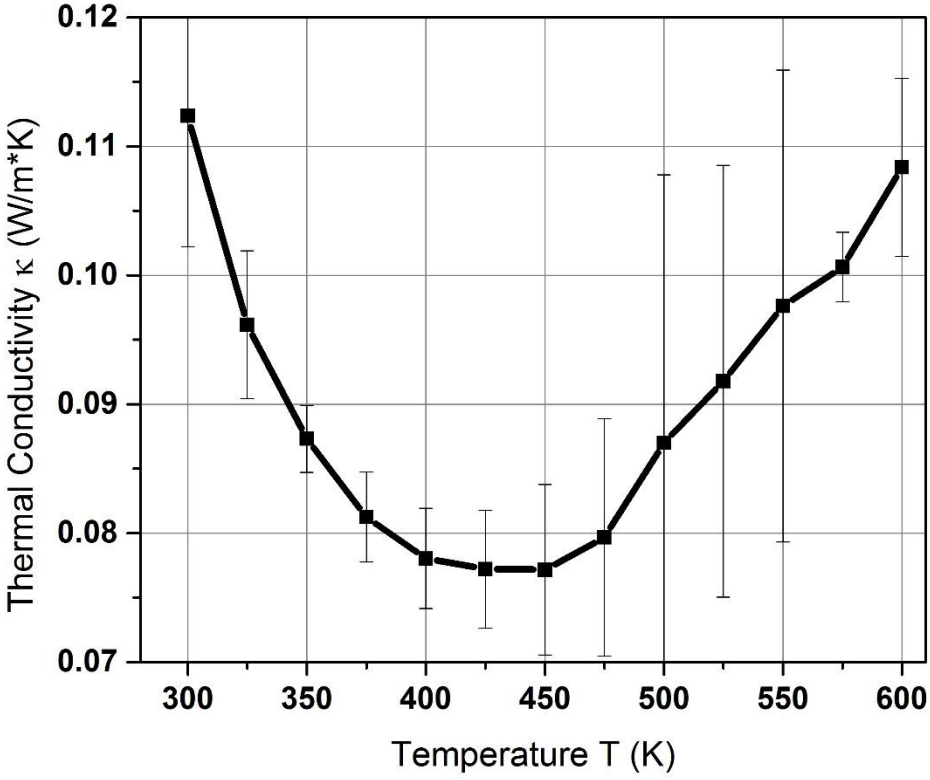

Fig. 26 Calculated thermal conductivity of In-doped PbTe as a function of temperature.

Fig 25 compares the thermovoltage, V, between the 0.1at.% In and the other indium-doped PbTe sample that was doped at $2.9x10^{20}cm^{-3}$, or 0.3at.%In. It is observed that the voltage for the latter sample possesses a thermovoltage almost double that of the sample doped at 0.1at.%In. When placed in a Quantum Design Physical Property System (PPMS) the electron concentration for the PbTe sample doped at $2.9x10^{20}cm^{-3}$ possessed an electron concentration of $4x10^{18}cm^{-3}$ at a magnetic field at 0.5T. The sample doped to 0.1at.%In encompassed an electron concentration of $4.8x10^{16}cm^{-3}$ again at 0.5T. Notice

that the 0.1at% In sample's electron concentration is two orders of magnitude away from the saturation point (~3-5x$10^{18}$$cm^{-3}$).

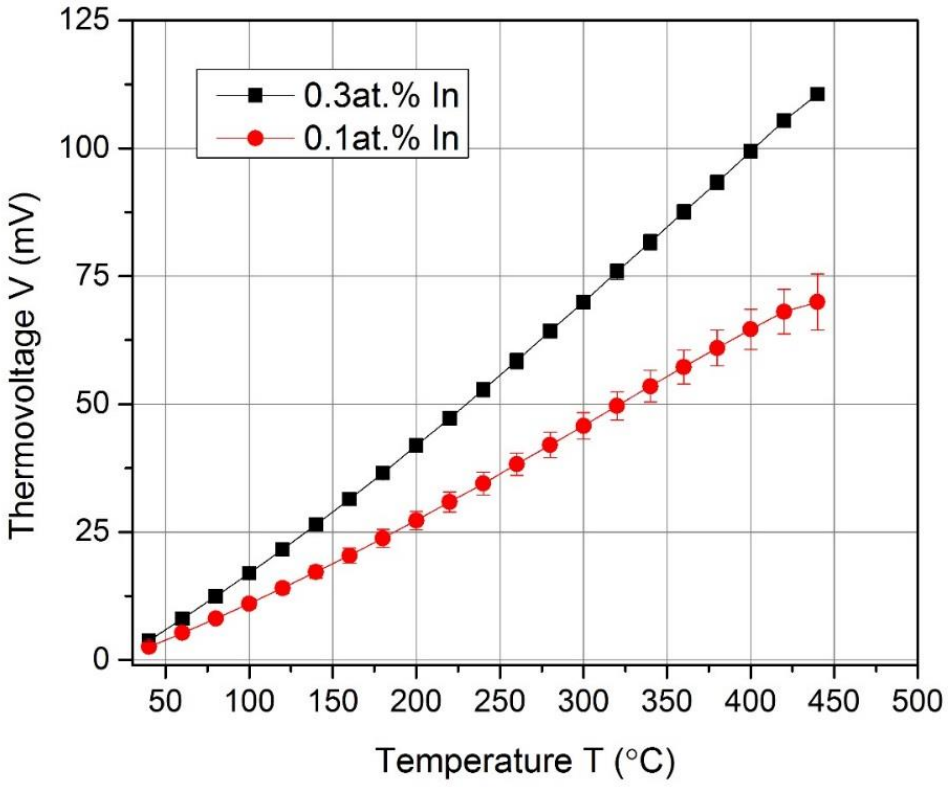

Fig. 27 The thermovoltage as a function of temperature for In-Doped PbTe sampled doped with 4. 5x$10^{20}$$cm^{-3}$ and 0.1at.% In.

CHAPTER VI

Discussion

6.1 Iodine Doped and Indium Doped PbTe Comparison

The behavior of I-doped PbTe and In-doped PbTe characteristics, for the most part, do not resemble each other. Fig 28 shows that the thermovoltage of the 0.3 at.% In-doped sample had a higher thermovoltage than the I-doped sample. The In-doped sample reached a maximum thermovoltage of ~110mV where the I-doped sample reached a thermovoltage of ~66mV.

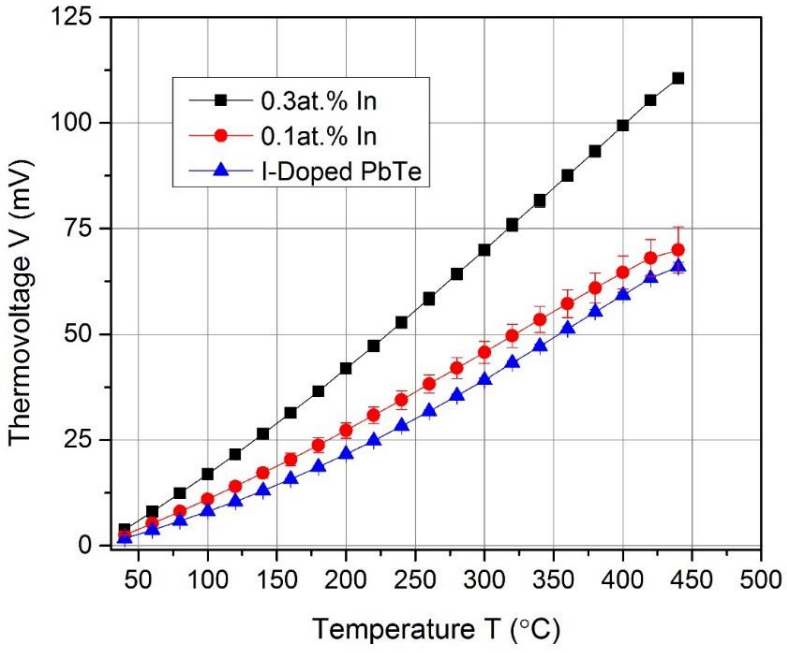

Fig. 28 Thermovoltage for both In-doped samples and the I-doped sample.

It appears that the thermovoltage of the 0.3at% In sample could continue to increase while the 0.1at.% In and the I-doped sample appear to begin leveling off.

Combining the voltage with the current and computing the power density, P_D, for all three of the samples is given in Fig 29.

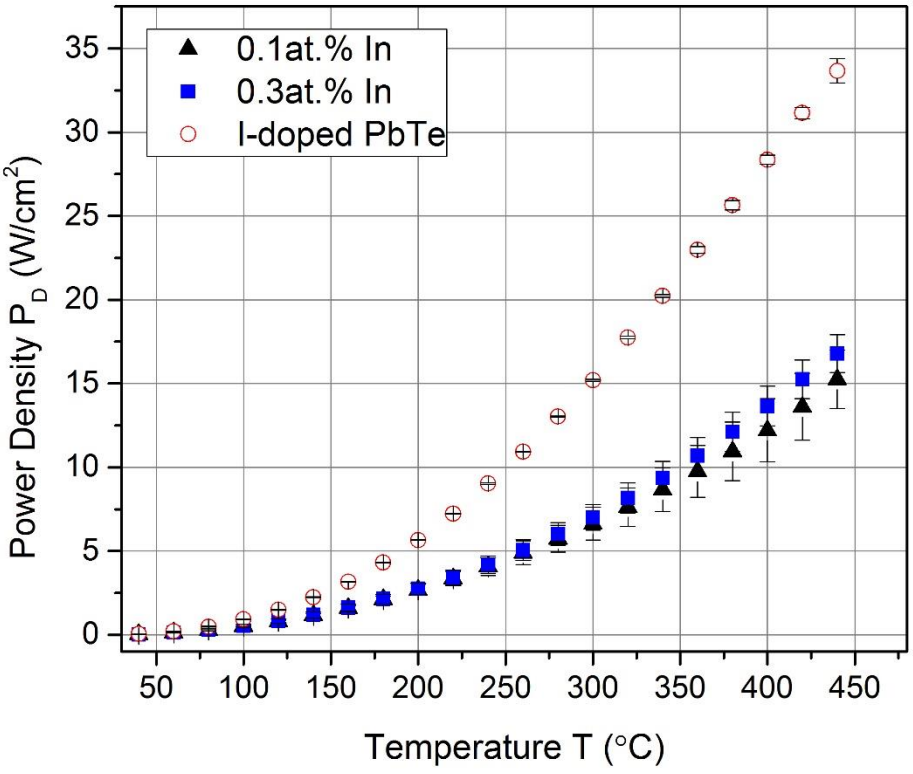

Fig. 29 Power density of the three samples as a function of temperature.

Despite the thermovoltage of the I-doped PbTe being slightly higher than half of the thermovoltage of the 0.3at.% In, the power density for the I-doped PbTe is nearly

double that of the In-doped sample. This large increase is due to the increase of current as can be seen in eq. 6.2.

Observing Fig. 32 it can be determined that I-doped PbTe possessed a significantly higher thermal conductivity than the In-doped sample. The I-doped sample had an electrical conductivity of ~1500 S/cm at 600K compared to the In-sample with an electrical conductivity of ~80 S/cm. The electrical conductivity of both samples were decreasing as temperature increased. This decrease is a result of the mobility falling as temperature increases and could be a result of more acoustical phonon activation. This large difference between the I-doped and In-doped electrical conductivity could contribute to the increase of the power factor for the I-doped sample thus increasing the total power output.

The FET gate mentioned earlier was used at 440°C for both samples. The I-doped sample had a measured maximum output power density of 8.83 W/cm^2 and the In-doped sample had a power density of 4.07 W/cm^2.

The electron concentration for the I-doped sample slightly decreases as temperature increases, a result of the ionization of minority carriers, while the electron concentration for the In-doped increases with temperature.

One chip from three identical wafers was used to measure the Seebeck coefficient for the indium and iodine doped samples. To account for the Seebeck effect of the Ni tabs, a small value of $12x10^{-6}/K$ was subtracted from each voltage value. Below are the

Seebeck coefficients for these samples in the temperature range 300K-470K.

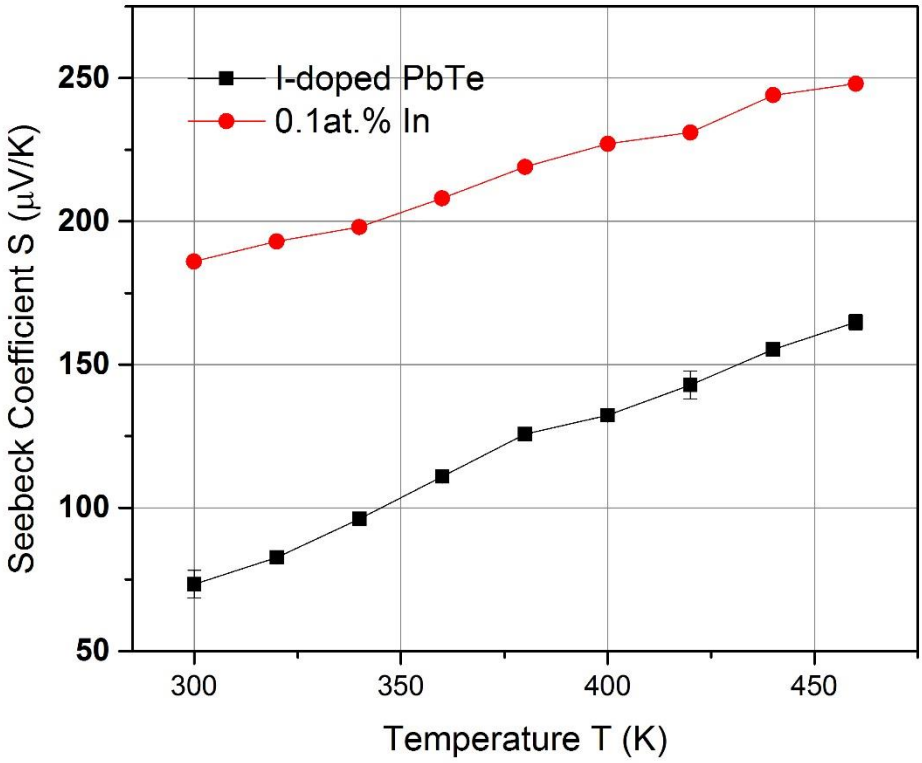

Fig. 30 Seebeck Coefficient for I-doped and In-doped samples.

The Seebeck coefficient for the indium doped sample is much higher than that of the iodine doped sample. With these values the power factor can be determined by using the following equation

$$P.F. = S^2\sigma \tag{7.1}$$

where S is the Seebeck coefficient and σ is the electrical conductivity. The power factor serves as an indicator of the thermoelectric efficiency with respect to the previously mentioned electronic properties.

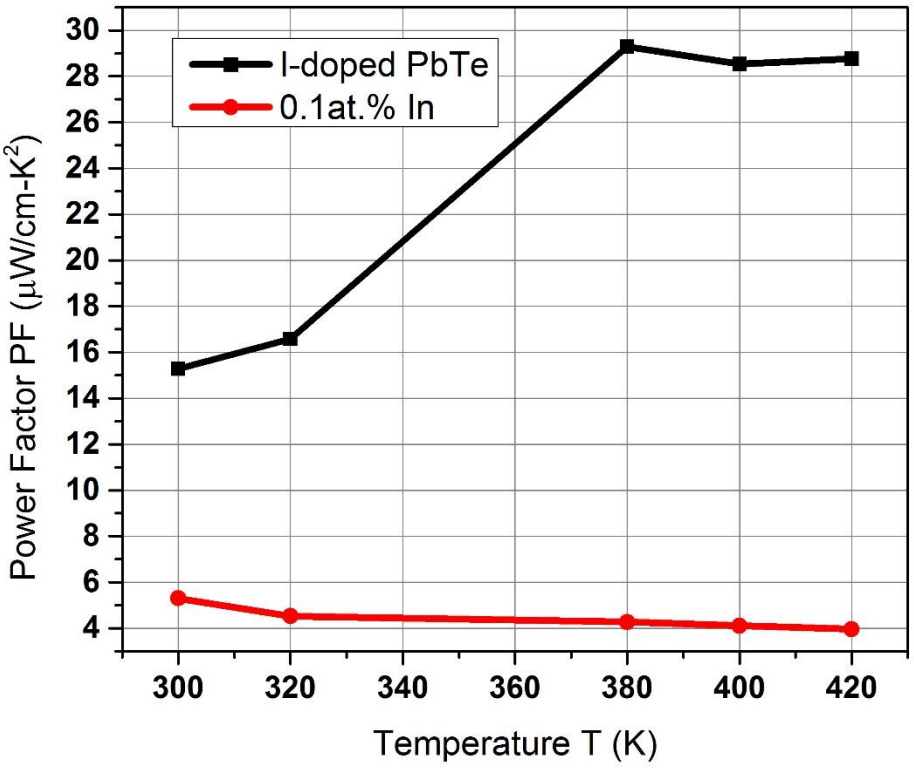

Fig. 31 Power factor as a function of temperature as calculated from S and σ, for the In-doped and I-doped samples.

Fig. 31 displays the power factor for both samples. The In-doped sample seems to remain constant while the iodine doped sample increases.

The measured thermal conductivity, κ, of both samples is shown in Fig. 32. The temperature range for the thermal conductivity is 320K-420K due to the inability of the apparatus to achieve temperatures greater than 420K.

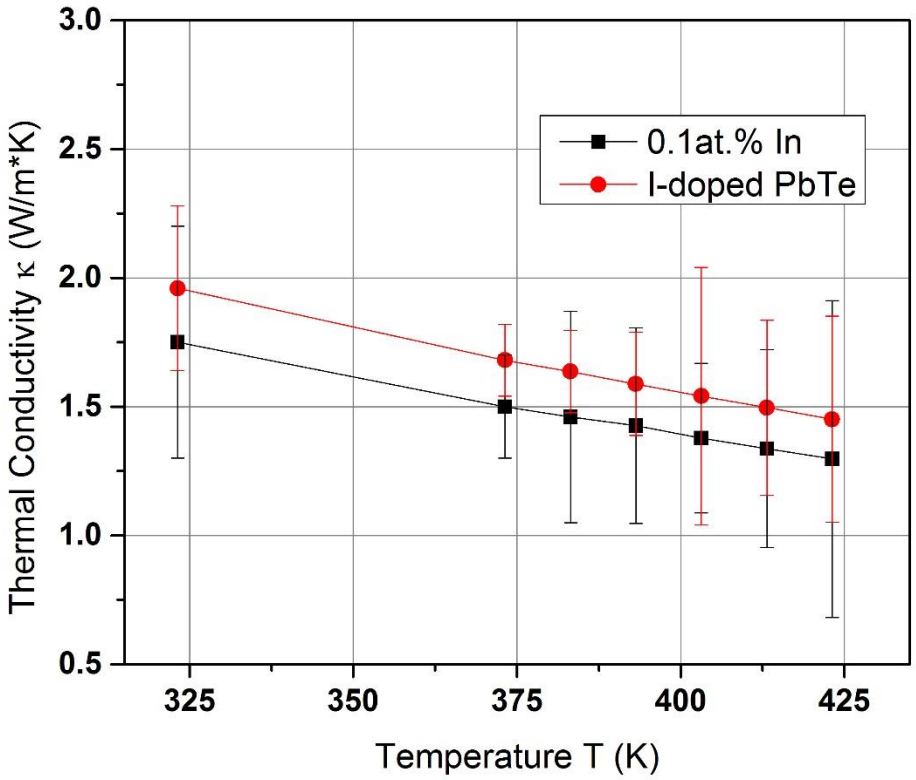

Fig. 32 Thermal conductivity of the iodine and indium doped samples.

From the above data, the values for the thermoelectric figure of merit can be computed by dividing the thermal conductivity by the power factor. The figure of merit ZT for the temperature range of 320-420K is shown in Fig.33. It is observed that the thermoelectric figure of merit for the I-doped PbTe is greater than that of the In-doped sample. The ZT for the indium doped sample remains stagnant in the measured temperature range while the iodine sample increases.

This is opposite to what was expected of the indium doped PbTe samples. Recall that the Z values were expected to be larger for indium doped PbTe. This low value could possibly be explained by deviating from the original crystal growth methodology.

The average values of the Seebeck, thermal conductivity, and electrical conductivity for both samples were used to compute the thermoelectric figure of merit and is plotted in Fig. 33.

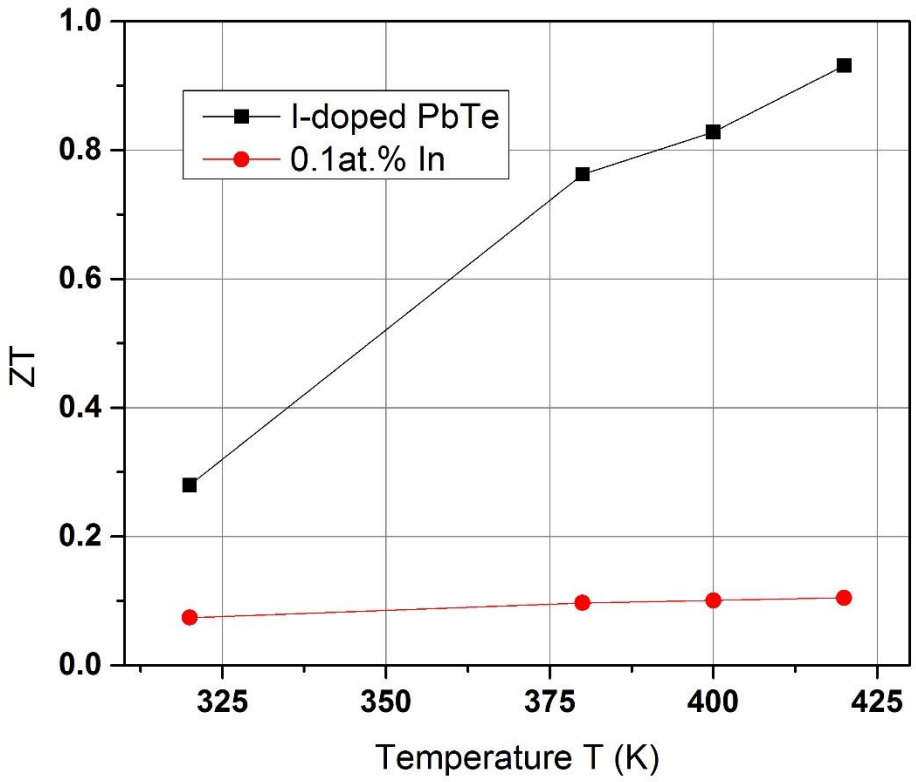

Fig. 33 The measured thermoelectric figure of merit for the iodine and indium doped samples.

6.2 Conclusion

Despite the In doped PbTe initially possessing a lower thermal conductivity and a high Seebeck coefficient, the iodine thermoelectric figure of merit managed to be greater than that of the indium doped sample. Further research is needed to compare the ZT values for both material at higher temperatures. With the provided data it is concluded that for our method of crystal growth, the thermoelectric performance of the iodine doped sample significantly outperformed the indium doped sample.

APPENDIX A

NOMENCLATURE

Symbol	Units	Description
A	mm^2	Area
e	C	Electron charge, $1.602x10^{-9}$ C
E	J or eV	Energy
F	N	Force
I,J	A	Current
k_B	J/K	Boltzmann Constant, $1.38065x10^{-23}$ J/K
m_e	kg	Electron Mass, $9.109x10^{-31}$ kg
ZT	---	Figure of Merit
S	$mV/m^2 \cdot K$	Seebeck Coefficient
κ	$W/m^2 \cdot K$	Thermal Conductivity
ρ	$m\Omega \cdot mm$	Electrical Resistivity
μ	$cm^2/N \cdot s$	Hall Mobilty

REFERENCES

[1] L. A. Fisk, *Science*, **309**, 2016 (2005)

[2] H. J. Goldsmid, Electronic Refrigeration (Pion Limited 1986).

[3] Yanzhong, Pei. "Low Effective Mass Leading to High Thermoelectric Performance." n.d.: 1.

[4] Dashevsky, Z. "Themoelectric efficiency in graded indium-doped PbTe crystals." 2002

[5] Gelbstein, Y. "High performance n-type PbTe-based materials for thermoelectric applications." *Physica B*, 2005.

[6] Snyder, J. (2008). Small thermoelectric generators. *The Electrochemical Society Interface*, 54-56.

[7] Haman, T.C. *Science*, 2002: 2229.

[8] Pollock, D. D. (1993). *Physical properties of materials for engineers*.

[9] Pollock, Daniel D. *Thermoelectricity, Theory, Thermometry, Tool.* 1985.

[10] *Brief History of Thermoelectrics.* n.d. http://thermoelectrics.caltech.edu/thermoelectrics/history.html.

[11] G. Jeffrey Snyder, Eric S. Toberer, Complex thermoelectric materials, Natur materials 7 (200*)

[12] G. S. Nolas, J. Sharp, H. J. Goldsmid, Thermoelectrics Basic Principles and New a. Materials Developments (Springer)

[13] Tsang, Y., Cohen, Marvin. "Calculation of the Temperature Dependence of the Energy Gaps in PbTe and SnTe.

[14] Shchennikov, V.V., Ovsyannikov, S.V., et al. "Thermopower of Lead Chalcogenides at High Pressures"

[15] Patrick Taylor, Jay Maddux, *et al.*: "Measurement of thermal conductivity using stead-state isothermal conditions and validation by comparison with thermoelectric device performance."

[16] Yu Ravich, B. A. Efimova: Semiconducting Lead Chalcogenides (Plenum Press, New York, New York.

[17] P.J. Taylor, W.A. Jesser, F.D. Rosi, Z. Derzko, Semicon. Sci. Technol., Vol. 12 p. 443 (1997)

[18] Garcia, A. R., & , et al.: (2013). Development and experimental validation of a thermoelectric test bench for laboratory lessons. *Journal of Technology and Science Education*, *3*(3)

[19] Dariel, M.P. "Carrier concentration gradient generated in p-type PbTe crystals by unidirectional solidification."*Journal of Crystal Growth*.

[20] Scolfaro, L.M.R. "Lattice contribution to the high dielectric constant of PbTe." *Physical Review B 87*, 2013.